

Pairing and superfluidity of nucleons in neutron stars

A. Gezerlis,^{1,2,3} C. J. Pethick,^{4,5} and A. Schwenk^{2,3}

¹Department of Physics, University of Guelph, Guelph,
Ontario, N1G 2W1, Canada

²Institut für Kernphysik, Technische Universität Darmstadt,
D-64289 Darmstadt, Germany

³ExtreMe Matter Institute EMMI, GSI Helmholtzzentrum für
Schwerionenforschung GmbH, D-64291 Darmstadt, Germany

⁴The Niels Bohr International Academy, The Niels Bohr Institute,
University of Copenhagen, Blegdamsvej 17, DK-2100 Copenhagen Ø,
Denmark

⁵NORDITA, KTH Royal Institute of Technology and Stockholm Uni-
versity, Roslagstullsbacken 23, SE-106 91 Stockholm, Sweden

April 15, 2015

“Our life is frittered away by detail. . . . Simplify, simplify.”
Henry David Thoreau, Walden.

Abstract

We survey the current status of understanding of pairing and superfluidity of neutrons and protons in neutron stars from a theoretical perspective, with emphasis on basic physical properties. During the past two decades, the blossoming of the field of ultracold atomic gases and the development of quantum Monte Carlo methods for solving the many-body problem have been two important sources of inspiration, and we shall describe how these have given insight into neutron pairing gaps. The equilibrium properties and collective oscillations of the inner crust of neutron stars, where neutrons paired in a 1S_0 state coexist with a lattice of neutron-rich nuclei, are also described. While pairing gaps are well understood at densities less than one tenth of the nuclear saturation density, significant uncertainties exist at higher densities due to the complicated nature of nucleon-nucleon interactions, the difficulty of solving the many-body problem under these conditions, and the increasing importance of many-nucleon interactions. We also touch more briefly on the subject of pairing of neutrons in other angular momentum states, specifically the 3P_2 state, as well as pairing of protons.

Keywords: Neutron matter, superfluidity, neutron stars, induced interactions, quantum Monte Carlo, atomic gases, collective modes

Contents

1	Introduction	3
1.1	Preamble and history	3
1.2	BCS theory	6
2	Dilute neutron gas	8
2.1	Induced interactions	10
2.2	Comparison with ultracold atomic gases	14
3	Microscopic calculations of pairing gaps	16
3.1	BCS approximation	16
3.2	Low densities	18
3.3	Higher densities	23
3.4	3P_2 pairing of neutrons	26
3.5	Proton pairing	27
4	The inner crust	28
4.1	Static properties	28
4.2	Hydrodynamic equations	29
4.3	Long-wavelength collective modes	33
4.4	Band structure and the neutron superfluid density	37
5	Conclusion	42
	References	43

1 Introduction

1.1 Preamble and history

In neutron stars one finds reservoirs of high-density fermions that are among the largest in the Universe and, because of the strong nucleon–nucleon interaction, a number of different phases can occur. Understanding properties of these phases is necessary to interpret observations of neutron stars, which are becoming increasingly more detailed. Temperatures in the interiors of neutron stars fall below a billion degrees Kelvin less than about one year after the birth of the star. Such temperatures may appear high, but they are low compared with the characteristic energies such as the Fermi energy, which in matter at nuclear density are typically ~ 10 – 100 MeV, corresponding to temperatures of order 10^{11} – 10^{12} K. Thus the effects of quantum degeneracy are important.

This chapter is devoted to pairing of neutrons and of protons in neutron stars at densities of order the saturation density of nuclei and below. The primary focus is on basic physical effects, on connections to other physical systems, and on topics where there has been significant recent progress. The bibliography is illustrative rather than exhaustive. Applications to observed neutron star phenomena are considered in another contribution to this volume [1]. For earlier reviews we refer to Refs. [2, 3].

Immediately after the Bardeen-Cooper-Schrieffer (BCS) theory of superconductivity was proposed, Bohr, Mottelson, and Pines [4] showed that the excitation energies of the lowest lying non-collective states of nuclei were significantly larger than could be accounted for on the basis of an independent-particle model. They proposed an analogy between the low-lying spectra of atomic nuclei and that of a superconducting metal and argued that pairing between nucleons could account for a number of features of nuclei. This idea was quickly followed up and led to profound insights into properties of nuclei (see, e.g., Ref. [5]). One of the manifestations of pairing in nuclei is a reduction of the moment of inertia of the nucleus, which results in an increase in the spacing of rotational levels compared with what would be expected for a rigid body. In an early paper on this subject, Migdal remarked in passing “We note that the superfluidity of nuclear matter can lead to interesting macroscopic phenomena if stars with neutron cores exist. Such a star would be in a superfluid state with a transition temperature corresponding to 1 MeV.” [6]. As we shall describe in greater detail in subsequent sections, Migdal’s comment was remarkably prescient. A few years later, Ginzburg and Kirzhnits [7, 8] estimated pairing gaps and pointed to a number of consequences of superfluidity in neutron stars. Properties of vortex lines in superfluid neutrons were

considered by Baym et al. [9], who also argued that superfluid protons would behave as a Type II superconductor, in which magnetic flux would penetrate the medium in the form of quantized flux lines.

Following the discovery of neutron stars, Hoffberg et al. [10] calculated gaps for neutron matter within the BCS theory using a separable nucleon-nucleon interaction that had been fitted to two-nucleon scattering data. Their calculations predicted a pairing gap for neutrons in the 1S_0 state¹ that first rose with increasing density, reached a maximum of roughly 3 MeV at a density of about $n_s/10$, where $n_s \approx 0.16 \text{ fm}^{-3}$ is the saturation density of nuclear matter with equal numbers of neutrons and protons, a density typical of the interiors of heavy nuclei. With further increase in density, the gap dropped and vanished at a density somewhat below n_s . At that density it had already become favorable for neutrons to pair in the 3P_2 state, in which the pairs have unit orbital angular momentum, unit spin, and total angular momentum 2. That the 3P_2 state has a more attractive interaction than the other 3P states is due to the fact that the spin-orbit interaction is attractive for nucleons. This situation is to be contrasted with that in atomic physics, where the spin-orbit interaction is repulsive. The 3P_2 gap increased to about 0.5 MeV at a density of around $2n_s$ and dropped at higher densities. The qualitative behavior of the gaps may be understood in terms of the measured phase shifts for nucleon-nucleon interactions, which are displayed in Fig. 1. A positive phase shift corresponds to an attractive interaction between neutrons, and therefore at low k , which corresponds to low Fermi momentum and low density, the most attractive channel is 1S_0 , while at higher densities the interaction in the 3P_2 channel is more attractive.

In what we (in common with most of the literature in nuclear physics) refer to as the BCS approximation, the gap is calculated by solving the BCS equation with the free-space nucleon-nucleon interaction and for free particles in intermediate states in the scattering process: the effects of the neutron medium on the normal state excitations and the pairing interaction are neglected.² A variety of techniques have been used to include effects beyond the BCS approximation in calculations of neutron pairing, and they typically predict a reduction of the pairing gap by a factor of 2 or more. The earliest estimates of the effects of the medium were made with variational methods involv-

¹We use the standard spectroscopic notation $^{2S+1}L_J$ to specify the angular momentum state of the paired particles. Here S is the total spin of the two particles, L is the orbital angular momentum of their relative motion, and J is the total angular momentum.

²We make the definition of the phrase ‘‘BCS approximation’’ explicit because, in the physics literature, there are a number of usages of the phrase, among which is the BCS schematic model for the interaction, in which one assumes that the interaction matrix element is constant for a range of momentum states in the vicinity of the Fermi surface.

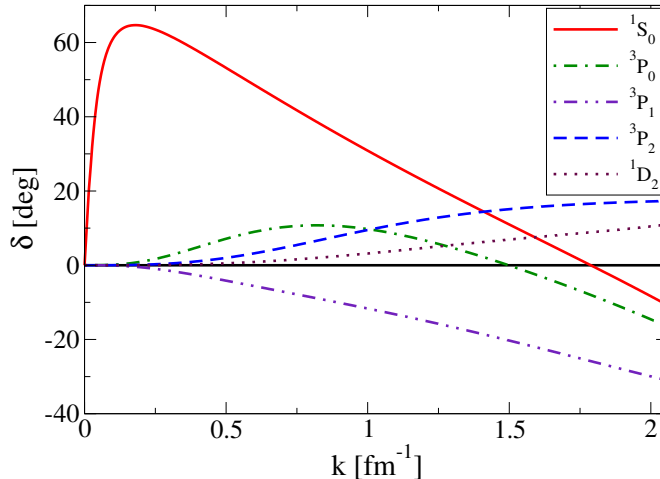


Figure 1: Scattering phase shifts as a function of the wave number of a nucleon in the center of mass frame based on the Nijmegen partial-wave analysis of experimental data [11]. The results are for neutron-proton scattering but, due to the fact that isospin symmetry is only weakly broken, they provide a good approximation for neutron-neutron scattering. Recall that a positive phase shift corresponds to an attractive interaction.

ing wave functions that include the effects of correlations [12] and with the use of methods inspired by diagrammatic perturbation theory [13].

In neutron stars, S-wave pairing is predicted to occur at subnuclear densities and the bulk properties of neutron matter are an important ingredient in understanding matter at such densities despite the fact that the neutrons coexist with a lattice of nuclei and an electron gas. Two developments over the past two decades have been important for understanding this region. One is the increasing power of quantum Monte Carlo methods to make accurate predictions based on the underlying interactions between individual nucleons. The second is the experimental realization of atomic gases at ultralow temperatures, where quantum effects manifest themselves.

The remainder of this chapter is organized as follows: in Sec. 1.2 we describe the BCS theory and its application to the neutron liquid. In Sec. 2 we describe pairing in a dilute Fermi gas and show that the reduction of the pairing interaction due to screening by the medium gives rise to a suppression of the pairing gap even in the limit of very low densities. The analysis there provides valuable insight into the results of detailed many-body calculations for neutron matter. In addition, the physics of neutron matter is compared and contrasted with that of ultracold atomic gases. Microscopic calculations of gaps are described in Sec. 3; besides the ¹S₀ state in neutron matter, we

consider the $^3\text{P}_2$ state, and pairing of protons in the $^1\text{S}_0$ state. The inner crust of neutron stars, where superfluid neutrons coexist with a crystal lattice of neutron-rich nuclei and an electron gas, is the subject of Sec. 4. There we begin with calculations of static properties, before going on to describe a hydrodynamic approach to long-wavelength dynamics and collective modes, and the problem of determining the neutron superfluid density. Section 5 contains concluding remarks.

1.2 BCS theory

We begin by giving a brief overview of BCS theory mainly to establish notation. For an unpolarized system of spin-1/2 particles interacting via a two-body potential, the BCS wave function for the ground state includes pairing between particles in a spin-singlet state with zero orbital angular momentum or, equivalently, between particles with equal and opposite spin and momentum, and it has the form (see e.g. Refs. [14, 15])

$$|\psi_{BCS}\rangle = \prod_{\mathbf{k}} (u_{\mathbf{k}} + v_{\mathbf{k}} c_{\mathbf{k}\uparrow}^\dagger c_{-\mathbf{k}\downarrow}^\dagger) |0\rangle, \quad (1)$$

where the operator $c_{\mathbf{k}\sigma}^\dagger$ creates a particle with wave vector \mathbf{k} and spin projection $\sigma = \uparrow, \downarrow$ and $c_{\mathbf{k}\sigma}$ destroys one. The coefficients $u_{\mathbf{k}}$ and $v_{\mathbf{k}}$, which without loss of generality may be taken to be real and positive, satisfy the normalization condition

$$u_{\mathbf{k}}^2 + v_{\mathbf{k}}^2 = 1. \quad (2)$$

For the wave function (1) the probability of the single-particle state $\mathbf{k}\sigma$ being occupied is $v_{\mathbf{k}}^2$ and the probability that it is unoccupied is $u_{\mathbf{k}}^2 = 1 - v_{\mathbf{k}}^2$.

The wave function (1) is not an eigenstate of the number of particles, $\hat{N} = \sum_{\mathbf{k},\sigma} c_{\mathbf{k}\sigma}^\dagger c_{\mathbf{k}\sigma}$. Therefore it is convenient to work in the grand canonical ensemble, in which the average number of particles, \bar{N} , is fixed, the bar indicating an expectation value for the BCS wave function. The average particle number is given by

$$\bar{N} = \langle \hat{N} \rangle = \langle \psi_{BCS} | \sum_{\mathbf{k}} \left(c_{\mathbf{k}\uparrow}^\dagger c_{\mathbf{k}\uparrow} + c_{\mathbf{k}\downarrow}^\dagger c_{\mathbf{k}\downarrow} \right) | \psi_{BCS} \rangle = 2 \sum_{\mathbf{k}} v_{\mathbf{k}}^2. \quad (3)$$

In the BCS approximation, one calculates the expectation value of the Hamiltonian H for the wave function (1). Terms in the interaction energy that do not correspond to pairing correlations but rather to Hartree and Fock contributions, e.g., ones with factors of the form $v_{\mathbf{k}}^2 v_{\mathbf{k}'}^2$, are neglected and the result is

$$\langle H - \mu \hat{N} \rangle = 2 \sum_{\mathbf{k}} \xi(\mathbf{k}) v_{\mathbf{k}}^2 + \sum_{\mathbf{k}\mathbf{k}'} \langle \mathbf{k} | V | \mathbf{k}' \rangle u_{\mathbf{k}} v_{\mathbf{k}} u_{\mathbf{k}'} v_{\mathbf{k}'}, \quad (4)$$

where $\xi(\mathbf{k}) = \epsilon(\mathbf{k}) - \mu$, $\epsilon(\mathbf{k}) = \hbar^2 k^2 / 2m$ is the kinetic energy of a particle with wave vector \mathbf{k} , μ is the chemical potential, and $\langle \mathbf{k} | V | \mathbf{k}' \rangle$ is the matrix element of the interaction Hamiltonian between a two-body state with a pair of particles with opposite spin and wave vectors $\pm \mathbf{k}$ and a similar state in which the particles have wave vectors $\pm \mathbf{k}'$. Minimizing this expression subject to the normalization constraint (2) one obtains the so-called gap equation

$$\Delta(\mathbf{k}) = - \sum_{\mathbf{k}'} \langle \mathbf{k} | V | \mathbf{k}' \rangle \frac{\Delta(\mathbf{k}')}{2E(\mathbf{k}')}, \quad (5)$$

where the gap is given by the expression

$$\Delta(\mathbf{k}) = - \sum_{\mathbf{k}'} \langle \mathbf{k} | V | \mathbf{k}' \rangle u_{\mathbf{k}'} v_{\mathbf{k}'}. \quad (6)$$

Here $E(\mathbf{k}) = \sqrt{\xi(\mathbf{k})^2 + \Delta(\mathbf{k})^2}$ is the quasiparticle excitation energy and in terms of this one finds

$$u_{\mathbf{k}}^2 = \frac{1}{2} \left(1 + \frac{\xi(\mathbf{k})}{E(\mathbf{k})} \right) \quad \text{and} \quad v_{\mathbf{k}}^2 = \frac{1}{2} \left(1 - \frac{\xi(\mathbf{k})}{E(\mathbf{k})} \right). \quad (7)$$

The chemical potential is found by solving the gap equation together with the equation for the average particle number,

$$\langle N \rangle = \sum_{\mathbf{k}} \left[1 - \frac{\xi(\mathbf{k})}{E(\mathbf{k})} \right]. \quad (8)$$

Equations (5) and (8) can be decoupled when $\Delta/\mu \ll 1$, a condition that is not satisfied for the strongly paired systems discussed here (ultracold atomic gases with resonant interactions and neutrons at relatively low densities). Therefore, these two equations have to be solved self-consistently. The BCS approximation gives a good qualitative description of the pairing gap but, as we shall describe in following sections, there are quantitatively significant effects due to correlations in the medium.

For pairing in the 1S_0 state, the gap is independent of the direction of \mathbf{k} and Eq. (5) takes the form

$$\Delta(k) = - \frac{1}{\pi} \int_0^\infty dk' k'^2 \frac{V(k, k')}{E(k')} \Delta(k'), \quad (9)$$

where $V(k, k')$, the matrix element of the potential averaged over the angle between \mathbf{k} and \mathbf{k}' , is given by

$$V(k, k') = \int_0^\infty dr r^2 j_0(k'r) V(r) j_0(kr), \quad (10)$$

$j_0(kr)$ being the spherical Bessel function of zeroth order. Similarly, Eq. (8) may be written as an expression for the particle number density $n = \langle N \rangle / \Omega$, where Ω is the volume of the system:

$$n = \frac{1}{2\pi^2} \int_0^\infty dk k^2 \left(1 - \frac{\xi(k)}{E(k)} \right). \quad (11)$$

These new equations are one-dimensional, and thus easier to solve numerically. We have solved Eq. (9) together with Eq. (11) for the 1S_0 channel of the Argonne v_{18} potential [16], which contains a strong short-range repulsion. This calculation is simplified by transforming the problem into a quasilinear one, as described in Ref. [17]. We have also solved these equations for a potential $V(r) = B \operatorname{sech}^2(r/d)$ with the strength B and range parameter d tuned so that it describes cold atomic systems, for which the effective range is much shorter than the interparticle spacing (see Fig. 2) [18]. The main difference between the two is that for cold atoms the gap in terms of the Fermi energy $E_F = \hbar^2 k_F^2 / 2m$ continues to rise with increasing $k_F |a|$ and saturates at a finite, nonzero value for $k_F |a| \rightarrow \infty$ while for neutrons the gap drops to zero at a finite density. This latter effect is due to the fact that, as shown in Fig. 1, at large momenta the 1S_0 phase shift becomes negative, corresponding to a repulsive interaction.

2 Dilute neutron gas

At low energies, the effective interaction between two particles is determined by the S-wave scattering length, a . For two neutrons in a singlet spin state, the scattering length is -18.5 fm, which is large compared with the range of nuclear interactions, ~ 1 fm. For densities much less than $1/a^3 \sim 10^{-4}$ fm $^{-3}$, the leading interaction contributions to the properties of the system may be calculated in terms of an effective interaction of the form

$$U_0 = \frac{4\pi\hbar^2 a}{m} \quad (12)$$

in momentum space, which corresponds to a delta function in coordinate space. The study of dilute quantum gases, which dates back to the period when many-body theory was in rapid development in the 1950s and 1960s, has experienced a renaissance following the experimental realization of such systems with ultracold atoms [19]. This has led to considerable insight into the properties of neutron matter. The condition for a gas to be dilute is that the interparticle spacing, r_s , be large compared with the magnitude of the scattering length a of the particles or, since the Fermi wave number k_F is proportional

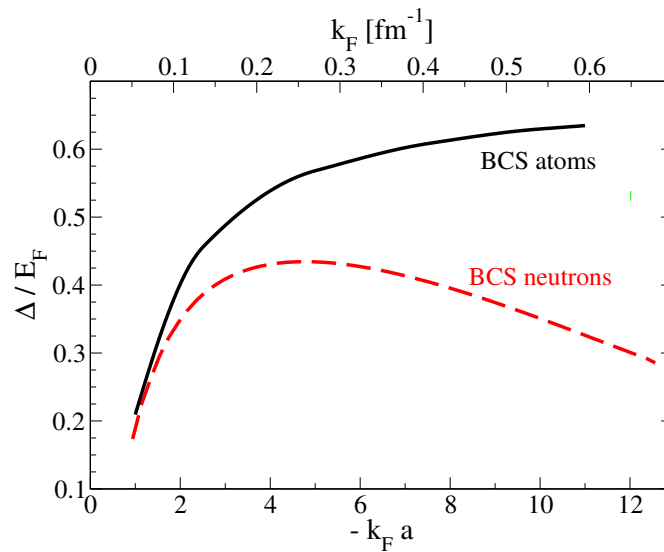


Figure 2: Pairing gap in the BCS approximation in terms of the Fermi energy $E_F = \hbar^2 k_F^2 / 2m$ versus $-k_F a$ for cold atoms and neutron matter (for details of the potentials used, see text). The upper scale is the Fermi wave number k_F for neutron matter when the scattering length is taken to have its experimentally determined value $a = -18.5$ fm. For $k_F |a| \lesssim 1$ the two results agree, which shows that, under these conditions, the gap is independent of the nonzero range of the neutron–neutron interaction.

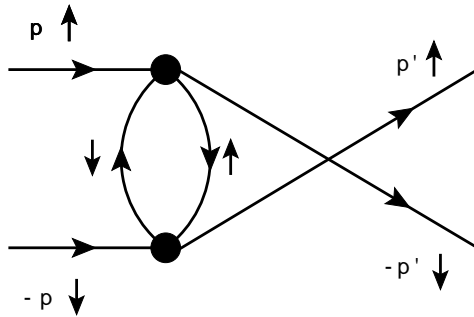


Figure 3: Diagrammatic representation of the simplest modification of the effective interaction due to the surrounding medium.

to $1/r_s$, this condition is equivalent to $k_F|a| \ll 1$. In a very important paper, which was overlooked for many years, Gor'kov and Melik-Barkhudarov studied the transition temperature and pairing gap for such a system [20] and we begin by explaining their calculation in physical terms [21].

In standard BCS theory (Sec. 1.2), one takes into account repeated scattering between a pair of particles via the free-space two-body interaction. If the interaction is eliminated in favor of the scattering length, one finds for a dilute Fermi gas with two spin components of equal mass and equal number densities for the pairing gap Δ_{BCS} at zero temperature the result

$$\Delta_{\text{BCS}} = \frac{8}{e^2} E_F e^{-1/N(E_F)|U_0|} \approx 1.083 E_F e^{-1/N(E_F)|U_0|}, \quad (13)$$

where the scattering length is taken to be negative. The quantity $N(E_F) = mk_F/(2\pi^2\hbar^2)$ is the density of states of a single spin species at the Fermi surface. Somewhat surprisingly, by systematically investigating the low-density limit, Gor'kov and Melik-Barkhudarov found

$$\Delta = \left(\frac{2}{e}\right)^{7/3} E_F e^{-1/N(E_F)|U_0|} \approx 0.489 E_F e^{-1/N(E_F)|U_0|}, \quad (14)$$

a factor $(4e)^{1/3} \approx 2.22$ smaller than the BCS value. The difference between the two results is due to the influence of the medium on the interaction between pairs of particles, as we shall now explain.

2.1 Induced interactions

In a dilute Fermi gas with a short-range interaction there is very little interaction between particles of the same spin because the Pauli principle hinders particles in the same spin state from coming close together. Consequently, the interaction may be taken to operate only

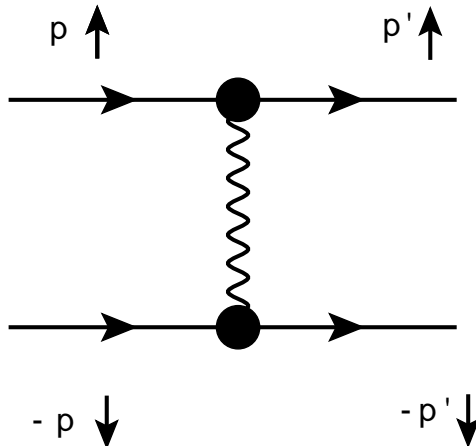


Figure 4: Diagrammatic representation of the induced interaction due to exchange of a density fluctuation in the surrounding medium.

between particles of opposite spin, in which case the simplest modification of the interaction is the screening process shown in Fig. 3, and its contribution for zero energy transfer between the particles is

$$U_{\text{ind}} = U_0^2 L(|\mathbf{p} + \mathbf{p}'|), \quad (15)$$

where

$$L(q) = N(E_F) \left[\frac{1}{2} + \frac{(1-w^2)}{4w} \ln \left| \frac{1+w}{1-w} \right| \right], \quad (16)$$

with $w = q/2p_F$, is the static Lindhard function familiar from the theory of screening in the electron gas and the Fermi momentum is given by $p_F = \hbar k_F$. For scattering of two particles on the Fermi surface, q is given by $2p_F \cos(\theta/2)$ and therefore when averaged over the angle θ between \mathbf{p} and \mathbf{p}' on the Fermi surface one finds

$$\langle U_{\text{ind}} \rangle = N(E_F) \frac{U_0^2}{3} (1 + 2 \ln 2) = 2N(E_F) U_0^2 \ln[(4e)^{1/3}], \quad (17)$$

where $\langle \dots \rangle$ denotes the average over the Fermi surface. On replacing the interaction U_0 in the BCS expression for the gap, Eq. (13), by U_0 plus the average of the induced interaction one finds to lowest order in the small parameter $N(E_F)U_0 = (2/\pi)k_F a$ that the gap is reduced by a factor $(4e)^{1/3}$, as we mentioned in Eq. (14) above.

Further insight may be obtained by analyzing the induced interaction in terms of exchange of excitations in the medium. A short-range interaction between fermions is described by the Hamiltonian

$$H_{\text{int}} = U_0 \int d^3r n_{\uparrow}(\mathbf{r}) n_{\downarrow}(\mathbf{r}) = \frac{U_0}{4} \int d^3r [n(\mathbf{r})^2 - n_s(\mathbf{r})^2], \quad (18)$$

where $n_{\uparrow}(\mathbf{r}) = \hat{\psi}_{\uparrow}^{\dagger}(\mathbf{r}) \hat{\psi}_{\uparrow}(\mathbf{r})$ and $n_{\downarrow}(\mathbf{r}) = \hat{\psi}_{\downarrow}^{\dagger}(\mathbf{r}) \hat{\psi}_{\downarrow}(\mathbf{r})$. The total number density is given by $n(\mathbf{r}) = n_{\uparrow}(\mathbf{r}) + n_{\downarrow}(\mathbf{r})$, and the spin density by

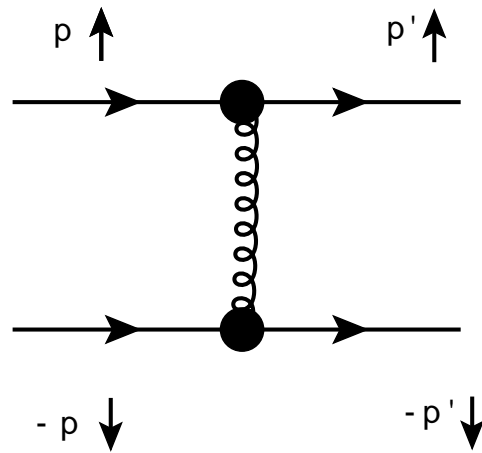


Figure 5: Diagrammatic representation of the induced interaction due to exchange of a spin fluctuation with spin projection $m_S = 0$ along the quantization axis.

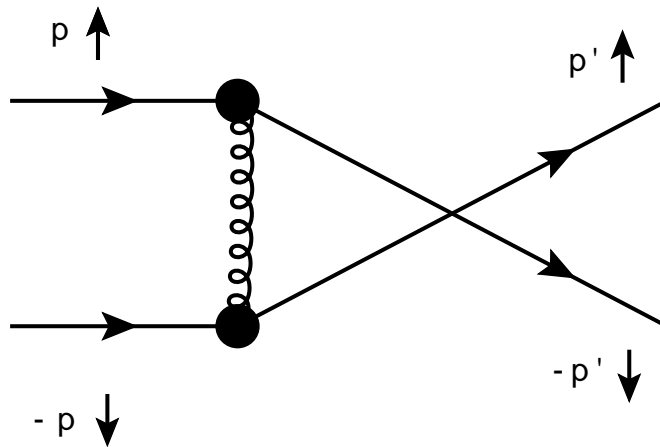


Figure 6: Diagrammatic representation of the induced interaction due to exchange of a spin fluctuation with spin projection $m_S = \pm 1$ along the quantization axis.

$n_s(\mathbf{r}) = n_\uparrow(\mathbf{r}) - n_\downarrow(\mathbf{r})$. Here $\hat{\psi}_\sigma^\dagger(\mathbf{r})$ is the operator that creates a particle of spin projection σ at point \mathbf{r} and $\hat{\psi}_\sigma(\mathbf{r})$ is the corresponding annihilation operator. A repulsive interaction between particles with opposite spin therefore leads to a repulsive interaction between particle densities and an attractive one between spin densities.

The existence of the medium changes the interaction between two particles: in addition to the direct interaction between two particles, there are contributions due to exchange of excitations in the medium. One of the best known examples of this is the attractive interaction between electrons due to exchange of lattice phonons, which we show schematically in Fig. 4. The wiggly line represents a density fluctuation in the medium, which in the case of lattice phonons is a well-defined mode of the system, but in a Fermi liquid corresponds to a collection of particle-hole pairs as well as any well-defined collective modes that may exist. In an interacting Fermi system, spin fluctuations can also be exchanged, as illustrated in Fig. 5, where the curly line represents a spin fluctuation. This term is repulsive, because particles with opposite spin couple to spin fluctuations with opposite signs. In a dilute Fermi gas, the contribution from exchange of density fluctuations is exactly cancelled by that from spin fluctuations because, first, the density–density response function (the wiggly line) and the spin-density–spin-density response functions are both equal to the Lindhard function L and the coupling of particles to spin and density fluctuations are equal in magnitude (see Eq. (18)). In Fig. 5 the spin fluctuation carries no net spin projection along the quantization axis ($m_S = 0$). However, it is also possible to exchange spin fluctuations with $m_S = \pm 1$, as shown in Fig. 6. This term is also repulsive since, while the matrix elements of the spin-raising and spin-lowering operators at the vertices have the same sign, in contrast to matrix elements for the $m_S = 0$ case, the interaction has the nature of an exchange term and therefore acquires an additional minus sign. In a more general model in which particles couple to fluctuations of both number density and spin density with matrix elements g_n and g_s which are independent of momentum transfer, the contribution of induced interactions to the averaged pairing interaction from diagrams like those in Figs. 4, 5 and 6 is

$$\langle U_{\text{ind}} \rangle = -g_n^2 \langle \chi_n \rangle + 3g_s^2 \langle \chi_s \rangle, \quad (19)$$

where χ_n and χ_s are the static density and spin-density propagators (the negative of the density–density and spin-density–spin-density response functions). The factor 3 in the spin-fluctuation term is due to the fact that the spin exchanged can lie in any of the three spatial directions. That spin fluctuations tend to suppress S-wave superconductivity in metals has been known since the pioneering paper of Berk and Schrieffer [22], but the mechanism is quite general.

In liquid ^3He the interaction between atoms induced by exchange of spin fluctuations is also responsible for the relative stability of the anisotropic superfluid phases, in which atoms are paired in P-wave states [23]. In nuclear matter, the fermions have four spin-isospin states and therefore the above discussion for two internal states needs to be extended. In the context of ultracold atomic gases, the effect of fluctuations in three-component systems has been investigated in Ref. [24] and these ideas could also be exploited to study, e.g., a proton impurity in a neutron gas with both spin states populated.

The effects of the medium on the pairing interaction are important even at very low densities because first, these contributions are of order $k_F a$ times the lowest-order contribution and, secondly, the gap depends exponentially on the inverse of the pairing interaction. The medium also affects the quasiparticle spectrum but this does not change the leading behavior of the gap on $k_F a$ since corrections to the spectrum (as reflected in, e.g., the effective mass) are of order $(k_F a)^2$.

2.2 Comparison with ultracold atomic gases

One of the remarkable features of nucleon–nucleon interactions is that they are close to resonant at low energy. This is reflected in the fact that the scattering lengths for nucleons are much greater in magnitude than the range of the nucleon–nucleon interaction, ~ 1 fm. For two neutrons in a singlet state, $a = -18.5$ fm. Expressed in other terms, the neutron–neutron interaction is almost, but not quite, strong enough to create a bound state of two neutrons, a dineutron. For a neutron and a proton, the scattering lengths are again large, with values -23.7 fm for the singlet state and $+5.4$ fm for the triplet state. The large, positive value for the triplet state is due to the interaction in that channel being sufficiently strong to form a bound state, the deuteron, which has a binding energy much smaller than the typical depth of nucleon–nucleon interactions. As a consequence of the existence of the bound state, the effective low-energy interaction is repulsive.

Beginning in the 1990s, much progress was made in studying experimentally the properties of cold atomic gases under degenerate conditions. One of the remarkable features of such gases is that interactions between atoms exhibit molecular resonances, whose energies can be tuned by, e.g., varying the external magnetic field. It is therefore possible to realize experimentally gases in which correlations are strong, in the sense that the magnitude of the scattering length is comparable to or greater than the interparticle spacing. At the 1999 conference on Recent Advances in Many-Body Theories, George Bertsch threw down the challenge of determining the properties of a Fermi system in which the magnitude of the scattering length is very much greater than

the interparticle spacing [25]. Under such conditions, the scattering length becomes an irrelevant parameter and the only length scale in the problem is the interparticle spacing, r_s . As a consequence, the only relevant quantum-mechanical energy scale for low-energy phenomena is $\hbar^2/2mr_s^2$, which for Fermi systems is equivalent to the Fermi energy. Thus, in this regime, the energy per particle and the pairing gap are given by universal numbers times E_F . Specifically, the pairing gap is calculated to be $0.5E_F$ [26].

Does low-density neutron matter provide a realization of this universal behavior to be expected for a strongly-interacting system with short-range interactions? At first sight, one might expect so: the density needed to achieve the condition $k_F|a| \gtrsim 1$ is not a problem, since this corresponds to densities of order 10^{-5} fm^{-3} . However, one can see, e.g., from the behavior of the gap in the BCS approximation for cold atoms as a function of $k_F|a|$ shown in Fig. 2, that the asymptotic behavior of the gap is achieved only for $k_F|a| \gtrsim 10$. However, the BCS gap for neutrons does not saturate, but begins to fall as $k_F|a|$ increases. The reason is that, for Fermi wave numbers of order $10/|a|$, scattering of neutrons is not well approximated by the expression in which only the scattering length enters, and it is necessary to take into account momentum-dependent terms. In the effective-range expansion, the 1S_0 phase shift is related to the scattering length and the effective range, r_e , by the expression

$$\cot \delta_0 = -\frac{1}{a} + \frac{1}{2}k^2 r_e + \dots \quad (20)$$

Since the effective range for neutrons is 2.7 fm, one sees that for $k_F \simeq 10/|a|$ the momentum-dependent terms must be included. To express this result in other terms, if the leading term ($-1/a$) in the effective-range expansion were sufficient, to achieve $k_F > 10/|a|$ would imply a phase shift of $\arctan 10 \approx 84^\circ$, while for neutron–neutron scattering the maximum phase shift is only 65° (see Fig. 1).³ For atomic systems, large values of the scattering length may be achieved by exploiting molecular resonances, so-called Fano–Feshbach resonances, near zero energy in the two-atom system. Such resonances are referred to as broad if the two-body scattering amplitude is well approximated by its zero energy value, and as narrow when it is not [27]. For low momenta the behavior of the neutron–neutron 1S_0 phase shift bears a resemblance to that for atomic systems with a narrow resonance (however, for a narrow resonance the effective range is negative).

³For neutrons, the effective-range approximation is good only for a limited range of momenta. If one retains only the first two terms in the expansion, the phase shift is always positive for a negative scattering length and a positive effective range (the situation for neutrons) while the observed phase shift (Fig. 1) changes sign. Thus the vanishing of the gap at higher densities cannot be understood in terms of the effective-range expression for the phase shift.

The overall picture of neutron matter that emerges is that at low densities, $n \ll 1/|a|^3$, the effects of interactions may be calculated from a low-density expansion. With increasing density, correlations initially become more important but for densities of order $1/(|a|r_e)^{3/2}$, the interaction between particles with momenta of order k_F becomes weaker, and the pairing gap becomes smaller. This has been exploited to calculate the energy of neutron matter at densities $n \sim n_s/10$ in a systematic expansion based on the scattering length and effective range [28]. While at low densities the interaction may be approximated by a simple S-wave one, at higher densities the spin-dependent terms and three-body contributions play an increasingly important role.

3 Microscopic calculations of pairing gaps

In this section, we describe microscopic calculations of pairing gaps in neutron matter.⁴ The simplest approach is to use the BCS approximation, in which the pairing interaction is taken to be the free-space nucleon–nucleon interaction and it is assumed that the single-particle energies are those of free particles. Although this approximation does not reproduce the correct weak-coupling result because, as discussed in Sec. 2.1, it does not include induced interactions, it does provide a useful benchmark, since it probes the dependence on the nucleon–nucleon interaction used. Guided by the insights from low densities and the comparison with ultracold atomic gases, we shall discuss our understanding of the 1S_0 pairing gap in neutron matter at low densities, focusing on quantum Monte Carlo calculations that provide a systematic approach at strong coupling. At higher densities the situation is less clear, and we shall provide a critical review of calculations of the 1S_0 pairing gap in neutron matter. Finally, we shall comment on the challenges involved in microscopic calculations of 3P_2 neutron pairing and of proton pairing in neutron stars.

3.1 BCS approximation

There are a number of two-body interactions that fit low-energy nucleon–nucleon scattering data and there is very good agreement between the gaps calculated with these interactions although their short-distance behaviors differ. The reason for the good agreement is that, for calculating gaps, the quantity that matters is the scattering amplitude at energies of order the Fermi energy, and this is strongly constrained by nucleon–nucleon scattering data for nucleon momenta in

⁴Since our aim is to provide a critical review of state-of-the-art calculations, we do not discuss the more historical results, for which we refer to Ref. [1].

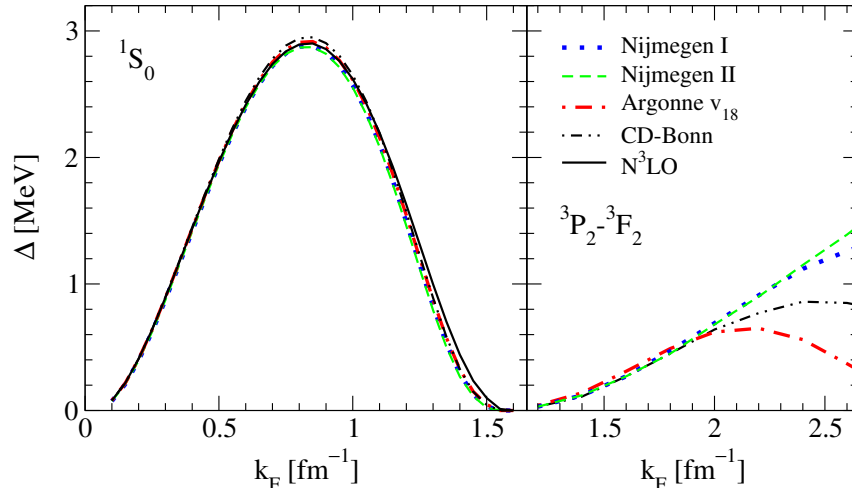


Figure 7: The 1S_0 (left panel) and 3P_2 – 3F_2 (right panel) pairing gaps Δ at the Fermi surface as a function of Fermi wave number k_F in neutron matter calculated in the BCS approximation for a number of charge-dependent nucleon–nucleon interactions that have been fitted to nucleon–nucleon scattering data. The potentials are specified according to the legend in the right panel. For details see Refs. [30] (left panel) and [33] (right panel).

the center-of-mass frame $k \lesssim 2 \text{ fm}^{-1}$ [29].⁵ For higher momenta, there is considerable model dependence, also because inelastic channels start to open up in nucleon–nucleon scattering, e.g., pion production for $k > 1.7 \text{ fm}^{-1}$.

Figure 7 shows the 1S_0 and 3P_2 – 3F_2 pairing gaps in neutron matter, obtained by solving the BCS gap equation with a free-particle spectrum for the normal state. At low densities (in the crust of neutron stars), neutrons form a 1S_0 superfluid. At higher densities, the S-wave interaction is repulsive and neutrons pair in the 3P_2 channel (with a small coupling to 3F_2 due to the tensor force). Figure 7 demonstrates that in the BCS approximation the 1S_0 gap is essentially independent of the nuclear interaction used [30]. This includes a very weak cutoff dependence for low-momentum interactions $V_{\text{low } k}$. The inclusion of the leading three-nucleon forces in chiral effective field theory gives a reduction of the 1S_0 BCS gap for Fermi wave numbers $k_F > 0.6 \text{ fm}^{-1}$ [31]. This reduction becomes significant for densities where the gap is decreasing and agrees qualitatively with results based on three-nucleon potential models (see, e.g., Ref. [32]). At low densities ($k_F \lesssim 0.6 \text{ fm}^{-1}$), 1S_0 pairing can therefore be calculated using only

⁵For simplicity, we shall frequently adopt the common practice of working in units in which $\hbar = 1$, in which case “momentum” and “wave number” become synonymous.

two-body interactions. At higher momenta, model potentials lead to different predictions for nucleon–nucleon scattering and this shows up prominently in Fig. 7 in the ${}^3\text{P}_2$ – ${}^3\text{F}_2$ gaps for Fermi wave numbers $k_F > 2 \text{ fm}^{-1}$ [33].

3.2 Low densities

At low densities, great progress has been made in calculating pairing gaps including medium effects using quantum Monte Carlo methods, a family of techniques used in condensed-matter physics, materials science, quantum chemistry, and nuclear physics to solve the quantum many-body problem using a stochastic approach (for a review see Ref. [34]). This is not the place for a detailed account of these methods but we hope to be able to give the reader a sense of the basic ideas behind them and of the ingredients needed to obtain reliable results. The methods are not restricted to weak potentials, for which perturbative methods are applicable, and state-of-the-art implementations of them lead to results for the energy that are accurate to within 1% of the value obtained from experiment or by exact diagonalization. For simplicity we shall limit ourselves to the case of zero temperature.

In the simplest of these methods, Variational Monte Carlo (VMC), one constructs for the N -particle system a trial wave function $|\psi_V\rangle$, which is a function of the $3N$ coordinates. The Hamiltonian H of the system contains contributions from the kinetic energy, and from two-body interactions (and possibly also three- and higher-body interactions), and one evaluates the integrals that occur in the expectation value of the Hamiltonian by stochastic sampling in the multi-dimensional space. From the Rayleigh-Ritz principle it follows that

$$E_{\text{VMC}} \equiv \frac{\langle \psi_V | H | \psi_V \rangle}{\langle \psi_V | \psi_V \rangle} \geq E_0, \quad (21)$$

where E_0 is the ground-state energy. By varying parameters in the trial wave function as well as its functional form, one can find the wave function that gives the lowest energy.

To see how one may further improve the wave function, consider the evolution of a state of the system in time. This is given by the equation

$$i\hbar \frac{\partial |\psi\rangle}{\partial t} = H |\psi\rangle. \quad (22)$$

One may expand the wave function in terms of energy eigenstates $|\psi_n\rangle$ of the Hamiltonian with eigenvalue E_n :

$$|\psi(t)\rangle = \sum_n c_n e^{-iE_n t/\hbar} |\psi_n\rangle, \quad (23)$$

where the c_n are coefficients independent of time. If one introduces the imaginary time variable $\tau = it$, one sees that with increasing τ , the component having the largest amplitude for large τ is that for the ground state. Thus, evolution of the wave function in imaginary time, which satisfies the equation

$$-\hbar \frac{\partial |\psi\rangle}{\partial \tau} = H|\psi\rangle, \quad (24)$$

systematically “purifies” the state by preferentially removing excited state contributions. This provides the basis for the Diffusion Monte Carlo (DMC) method, whose name reflects the fact that in coordinate space the kinetic energy operator is proportional to a sum of terms of the form ∇_i^2 , where i is the particle label, and therefore Eq. (24) resembles a diffusion equation in a $3N$ dimensional space.⁶ In practice, the starting point for the DMC method is frequently the wave function obtained from a VMC calculation.

Quantum Monte Carlo simulations for many-boson systems are, in principle, exact: an input wave function is employed but its only role is to reduce the statistical variance of the final result. Fermions are different due to the “fermion sign problem”. This arises because the ground state of the many-fermion problem corresponds to an excited state of the many-boson problem. When propagated in imaginary time, an initially antisymmetric wave function will, due to the statistical sampling, acquire components that are symmetric in the particle coordinates, and with time these grow and dominate the wave function: an initially fermionic wave function will thus evolve to the bosonic ground state. One method to circumvent this difficulty is to use a “fixed-node” approximation (for real wave functions) or a “constrained path” one (for complex wave functions), in which the stochastic evolution is artificially constrained [35]. For simplicity, we describe the method for real wave functions. Because of the antisymmetry of the spatial wave function, it has positive and negative regions, which are separated by nodal surfaces, which divide the multi-dimensional configuration space into a number of domains in which the wave function does not change sign. Within these domains, the evolution of the wave function corresponds to that of a many-boson problem. In the fixed-node approximation, one solves the evolution within each domain separately, keeping the positions of the nodal surfaces fixed. Unlike in the variational Monte Carlo approach, the wave function within each domain is not constrained to have a particular functional form. In the fixed-node approximation one needs to specify the nodal structure in some way and different choices lead to different ground-state energies.

⁶We caution the reader that there is no generally agreed upon nomenclature for the various Monte Carlo methods. To keep the discussion simple we shall not distinguish between the DMC method and the closely related Green’s Function Monte Carlo (GFMC) one.

Due to the computational demands, quantum Monte Carlo calculations can only be carried out for systems composed of (at most) a few hundred particles. To obtain results for the thermodynamic limit ($N \rightarrow \infty$, $\Omega \rightarrow \infty$, with $N/\Omega \rightarrow \text{constant}$, Ω being the volume of the system) the dependence of results on the particle number N must be carefully studied. Generally speaking, if the range of the interaction is small compared with the particle spacing, relatively few particles are needed to simulate the infinite system: e.g., for cold alkali atoms, where the particle spacing is $\sim 10^{-4}$ cm while the range of the interaction is of order 10^{-6} cm, there is essentially no variation when the particle number is increased above 40 (at zero temperature). The situation is different in the case of nuclear physics, since the range of the interaction (~ 1 fm) is comparable to the interparticle spacing.

A second complicating feature of nuclear physics is the spin and isospin dependence of the interaction. As a consequence of the rapid increase of the number of spin states with particle number, it is at present possible to study systems with 14 neutrons (or 12 nucleons if both neutrons and protons are present) [36].

A promising method, referred to as Auxiliary Field Diffusion Monte Carlo (AFDMC) [37] extends the stochastic evolution in coordinate space in the DMC method to spin-isospin space. This exploits the Hubbard–Stratonovich identity [38], which expresses a two-body operator as a sum of one-body operators interacting with random fields (the auxiliary fields in the name for the method) and integration over these fields. This integration is performed by Monte Carlo techniques analogous to those used to study the wave function in coordinate space. This method has the advantage that it can be used for larger systems but it suffers from the disadvantage that it does not give an upper bound on the energy.

In nuclear physics, a measure of the pairing gap is the systematic staggering of ground-state energies between nuclei with even numbers of neutrons (or protons) and those with odd numbers. Explicitly for the case of neutrons, in systems with even neutron number, N , all neutrons are paired, while for odd N one nucleon is not paired. The simplest way to express this pairing gap is in terms of the second difference

$$\Delta = (-1)^{N+1} \left\{ E(N) - \frac{1}{2} [E(N+1) + E(N-1)] \right\}, \quad (25)$$

where $E(N)$ is the ground-state energy of a system with N neutrons. Equation (25) may also be written in terms of the neutron separation energy,

$$S(N) = E(N) - E(N-1), \quad (26)$$

as

$$\Delta = \frac{(-1)^N}{2} [S(N+1) - S(N)]. \quad (27)$$

For large systems, this is equivalent to the definition in terms of the gap calculated within the BCS theory and extensions of it. In that approach, the minimum energy necessary to add an excitation to the system without changing the average particle number is Δ . Addition of a neutron to the ground state of a system with an even number of neutrons requires an energy $\mu + \Delta$, where μ is the chemical potential while to remove a particle requires an energy $-\mu + \Delta$. In both cases, one neutron is unpaired, so an extra energy Δ is required over and above the energy $\pm\mu$ required to add or remove a particle in the absence of pairing. One thus sees that the definition (25) is consistent with this. For applications to finite nuclei it is common to use higher-order difference expressions (see, e.g., [5, p. 17]) in order better to remove N -dependent contributions to the energy not due to pairing. However, in the case of unbound systems such as neutron matter, for which the dependence of the energy on particle number is smoother, this extra complication is unnecessary. Calculation of the pairing gap demands high accuracy for the calculations of the ground-state energies, since the pairing gap is small compared with the total energy of the system, $\sim NE_F$. Thus, to resolve the pairing gap, statistical errors must be reduced well below a level of $\sim \Delta/(NE_F)$. For low density neutron matter Δ/E_F can reach values as high as 0.4 and gaps can be calculated reliably, while in terrestrial superconductors Δ/E_F is much smaller and gaps cannot be extracted from numerical calculations of ground-state energies.

The simplest choice of a variational wave function, $|\psi_V\rangle$, for a normal gas is a Slater determinant, $|\psi_S\rangle$, of single-particle orbitals chosen according to the problem at hand: for neutron matter, they are plane waves. One typically also includes Jastrow correlation factors of the form $\prod_{i<j} f(r_{ij})$, possibly multiplied by an operator relevant to the interaction (in nuclear physics this includes spin-dependent central, spin-orbit, and tensor terms). Both the DMC and the AFDMC methods work with Jastrow factors that are only central: for neutron matter at low densities, where the interaction is mainly S-wave, this is expected to be a reasonable approximation. We noted earlier that the nodal structure of the variational wave function influences the final result. This also means that for functions $f(r)$ that are nodeless, the Jastrow term is relatively unimportant, except for controlling the statistical error.

For superfluid systems, pairing correlations strongly affect the nodal structure of the wave function and must be incorporated in the trial wave function from the start. The simplest choice is the BCS wave function (1), which may be written as

$$|\psi_{BCS}\rangle \propto \exp\left(\sum_{\mathbf{k}} (v_{\mathbf{k}}/u_{\mathbf{k}}) c_{\mathbf{k}\uparrow}^\dagger c_{-\mathbf{k}\downarrow}^\dagger\right) |0\rangle, \quad (28)$$

since a fermion creation or annihilation operator raised to a higher power than unity vanishes. Here $|0\rangle$ is the vacuum state. Thus, the component of this wave function with a definite (even) number of particles N may be written as

$$|\psi_{BCS,N}\rangle \propto \left(\sum_{\mathbf{k}} \alpha_{\mathbf{k}} c_{\mathbf{k}\uparrow}^{\dagger} c_{-\mathbf{k}\downarrow}^{\dagger} \right)^{N/2} |0\rangle, \quad (29)$$

where $\alpha_{\mathbf{k}} = v_{\mathbf{k}}/u_{\mathbf{k}}$. The wave function thus corresponds to the anti-symmetrized product of $N/2$ pairs of particles in the state specified in momentum space by the coefficients $\alpha_{\mathbf{k}}$. This wave function may be used as a trial function for general $\alpha_{\mathbf{k}}$, and the optimal form will generally be different from the BCS mean-field result. In coordinate space, the pair wave function is the Fourier transform of $\alpha_{\mathbf{k}}$.

We turn now to explicit calculations of gaps in neutron matter. One general point is that, due to the standard approaches to handling the fermion-sign problem (as detailed above), the nodal structure of the input wave function can really influence the final answer. For example, in the unitary Fermi gas $|\psi_S\rangle$ gives a ground-state energy that is 20% or more larger than that from $|\psi_{BCS,N}\rangle$ [39]. Even when a BCS-like wave function is used, there may be considerable dependence on the specific values chosen for $\alpha_{\mathbf{k}}$. This has, indeed, been the case for low-density neutron matter: since the interaction at such densities is dominated by its S-wave component, it is possible to apply both DMC and AFDMC, but the results obtained from the two approaches differed, due to the difference in input wave functions. Specifically, the DMC calculations in Ref. [18] used a variationally optimized wave function, leading to the results shown in Fig. 8. An important check on numerical calculations is provided by the analytic results of Gor'kov and Melik-Barkhudarov [20] described in Sec. 2 and also shown in the figure. The fact that such DMC calculations agree with the expected analytic behavior at the lowest densities, namely a suppression with respect to the BCS approximation value by a factor $(4e)^{-1/3} \approx 0.45$, increases one's confidence that they behave properly at intermediate densities. Another set of quantum Monte Carlo calculations used AFDMC along with $\alpha_{\mathbf{k}}$ calculated within the Correlated Basis Function (CBF) approach [40].⁷ This CBF wave function is ill-behaved since at very low densities it does not reproduce the results of Gor'kov and Melik-Barkhudarov. Since these CBF wave functions were used as input and define the nodal structure in the AFDMC computations, the AFDMC results also do not reproduce the correct low-density limit.

⁷The calculations included in addition a three-body interaction described by the Urbana IX potential but at low densities this should play no role, as discussed in Sec. 3.1

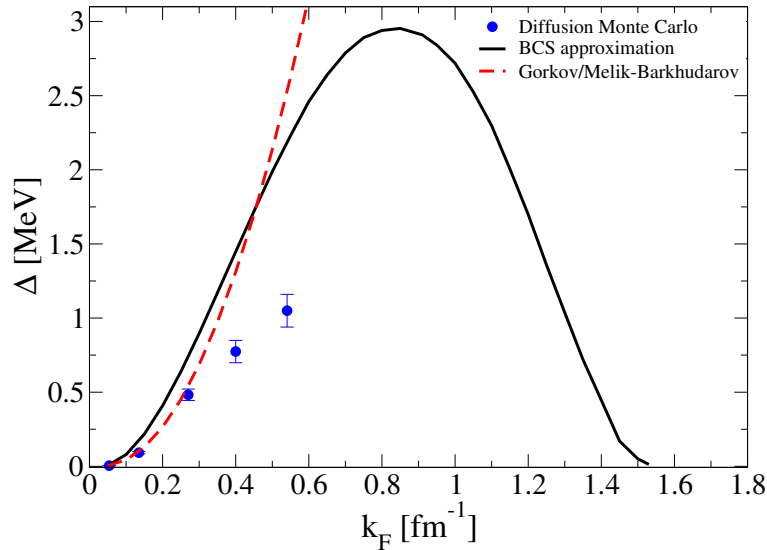


Figure 8: The 1S_0 pairing gap Δ as a function of Fermi wave number k_F in neutron matter. Results are shown for the BCS approximation (see Fig. 7), for the exact result in the low-density limit (Gor’kov/Melik-Barkhudarov) [20], which includes induced interactions, and for Diffusion Monte Carlo calculations of neutron matter [18].

The present status of calculations of gaps in neutron matter is that the situation at densities $\lesssim n_s/10$ is under good control, thanks to the analytical results in the low-density limit and quantum Monte Carlo methods: the physical reason for the suppression of the gap compared with the BCS approximation is the repulsive interaction induced by exchange of spin fluctuations. At higher densities there are larger uncertainties because additional terms in the neutron–neutron interaction become increasingly important and the increased density makes the extraction of gaps from energy differences more challenging.

In addition, three-neutron interactions begin to play a role but for neutron matter their effects are suppressed because configurations in which three neutrons are close together are unlikely, since at least two of the neutrons must be in the same spin state.

3.3 Higher densities

Figure 9 demonstrates that understanding many-body effects beyond the BCS approximation constitutes an important open problem at higher densities. All calculations shown in Fig. 9 are based on nucleon–nucleon interactions only, so the differences are due to truncations in the many-body calculations.

As discussed in Sec. 2.1, induced interactions due to screening and vertex corrections (creation of particle–hole pairs in intermediate

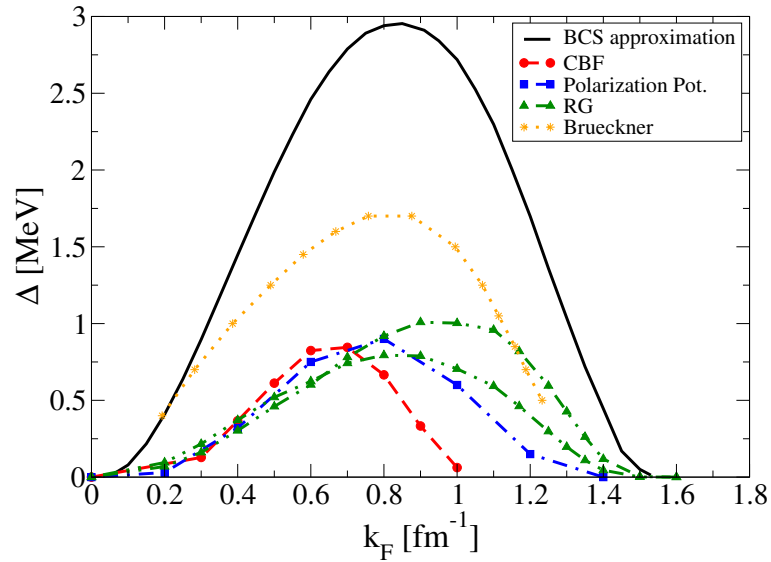


Figure 9: The 1S_0 pairing gap Δ at higher densities as a function of Fermi wave number k_F . Results are shown for the BCS approximation (see Fig. 7), for the method of Correlated Basis Functions (CBF) [12], for the polarization potential method, in which induced interactions are calculated in terms of pseudopotentials (Polarization Pot.) [13], for a calculation in which induced interactions in the particle-hole channels are calculated from a renormalization group (RG) approach [42], and for calculations based on Brueckner theory [46].

states) are crucial for a quantitative understanding of pairing gaps. They lead to a reduction of the 1S_0 gap that is significant even in the limit of low densities, $k_F|a| \rightarrow 0$ [20]:

$$\begin{aligned} \Delta &= \frac{8}{e^2} E_F \exp \left\{ \text{const.} \left(\begin{array}{c} \text{X} \\ \text{X} \\ \text{X} \\ \text{X} \end{array} + \begin{array}{c} \text{X} \\ \text{X} \\ \text{X} \\ \text{X} \end{array} + \begin{array}{c} \text{X} \\ \text{X} \\ \text{X} \\ \text{X} \end{array} + \dots \right)^{-1} \right\} \\ &= \frac{8}{e^2} E_F \exp \left(\frac{\pi}{2k_F a} + \ln[(4e)^{-1/3}] + \mathcal{O}(k_F a) \right). \end{aligned} \quad (30)$$

Because the exponent depends nonperturbatively on the pairing interaction, $\sim 1/g$, second-order induced interactions in the particle-hole channels lead to an $\mathcal{O}(1)$ correction to the pairing gap, $1/(g + C_2 g^2) \simeq 1/g - C_2$ in weak coupling, which leads to a reduction by a factor $(4e)^{-1/3} \approx 0.45$ in very low density neutron matter.

Following Shankar [41], Ref. [42] developed a nonperturbative renormalization group (RG) approach for neutron matter, where induced interactions in the particle-hole channels are generated by integrating out modes away from the Fermi surface. Starting from a nucleon–nucleon interaction, the solution to the RG equations in the particle-hole channels includes contributions from successive particle-hole momentum shells. The RG builds up many-body effects in a way similar to that in which the two-body parquet equations do, and efficiently includes induced interactions to low-lying states in the vicinity of the Fermi surface beyond a perturbative calculation. For momentum-independent interaction vertices, one can argue that the resummation of the particle-hole channel agrees with the truncated weak-coupling expansion: schematically after resumming the particle-hole channels: $1/(g + C_2 g^2 + \dots) \rightarrow (1 - C_2 g)/g = 1/g - C_2$. For a discussion in the context of the BCS-BEC crossover, see Refs. [43, 44].

The RG results [42] for the 1S_0 pairing gap based on a low-momentum interaction $V_{\text{low } k}$ are shown in Fig. 9. Induced interactions reduce the maximal gap by a factor ~ 3 to $\Delta \approx 0.8$ MeV. The two RG results shown in Fig. 9 provide a measure of the uncertainty due to an approximate treatment of the neutron self-energy. At low densities, the RG approach is consistent with the result $\Delta/\Delta_{\text{BCS}} \approx 0.45$ in the dilute limit, see also Ref. [45]. Note that the RG results give smaller gaps than the DMC results in Fig. 9. This is because the RG results are obtained from a weak-coupling BCS formula with pairing interaction from the particle-hole RG, and the weak-coupling BCS gaps are in reasonable agreement with the BCS approximation except at lower densities (see Fig. 8 in Ref. [42]).

Figure 9 shows that gaps calculated with Correlated Basis Function theory [12] and with induced interactions based on pseudopotentials [13] are in reasonable agreement with the RG results at lower densities, but there are considerable spreads in the density at which

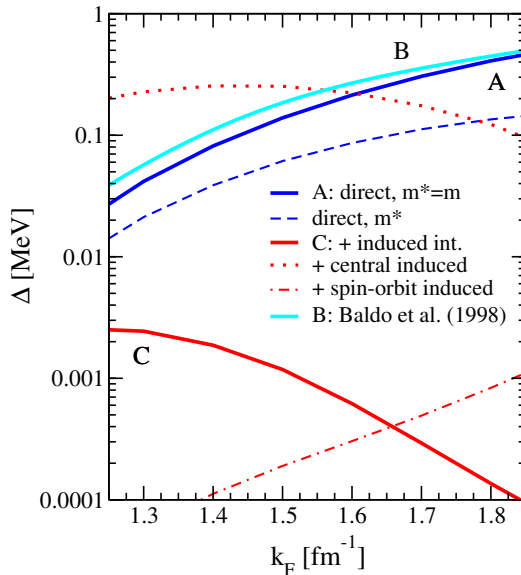


Figure 10: Angle-averaged 3P_2 pairing gap Δ versus Fermi wave number k_F in neutron matter. The calculations were made in the spirit of the BCS schematic model and for weak-coupling, and the gap is given by $\Delta = 2E_F \exp(1/N(E_F)V)$, where V is the pairing matrix element in the 3P_2 channel at the Fermi surface. The results are shown for the direct interaction only, both without and with corrections to the effective mass of the particles, and with the inclusion of second-order induced interactions in the pairing interaction. We also show the modification of the gap when only induced central or only induced spin-orbit effects are taken into account. For comparison, we give the results of Baldo *et al.* [33], which are obtained by solving the BCS gap equation in the coupled 3P_2 - 3F_2 channel for different free-space interactions (see also Fig. 7). For details see Ref. [51].

the gap is maximal and in the density at which it vanishes. In addition, in Fig. 9 we show results for the 1S_0 pairing gap in Brueckner theory [46], but they disagree with the known analytical result at low densities, where they predict a gap greater than Δ_{BCS} .

3.4 3P_2 pairing of neutrons

Noncentral spin-orbit and tensor interactions are crucial for 3P_2 superfluidity. In particular, without an attractive spin-orbit interaction, neutrons would form a 3P_0 superfluid, in which the spin and orbital angular momenta are anti-aligned, rather than the 3P_2 state, in which they are aligned.

Gaps calculated in the BCS approximation are shown in Fig. 7 and calculations of 3P_2 pairing including many-body effects are given in

Refs. [47, 48, 49, 50]. The ${}^3\text{P}_2$ gap is more sensitive to the pairing interaction than the S-wave gap, because the ${}^3\text{P}_2$ gap is very small compared to the Fermi energy. To date, there is only one (perturbative) calculation of non-central induced interactions [51]. This showed that, due to the coupling of the tensor and spin-orbit force to the strong spin-spin interaction (G_0), the tensor component of the quasiparticle interaction and the (P-wave) spin-orbit interaction are significantly reduced in neutron matter. As a result, ${}^3\text{P}_2$ gaps below 10 keV are possible in the interior of neutron stars, see Fig. 10 [51]. For ${}^3\text{P}_2$ pairing it is crucial to include non-central induced interactions, because P-wave pairing would be enhanced if only central induced interactions were included [50]. Note that these calculations do not include three-nucleon forces, which were found to increase the ${}^3\text{P}_2$ pairing gaps [47]. Understanding three-body forces is a frontier area in nuclear physics (for a recent review see Ref. [52]).

Typical interior temperatures of isolated neutron stars are on the order of $10^8 \text{ K} \approx 10 \text{ keV}$ and therefore it is possible to constrain the ${}^3\text{P}_2$ pairing gaps phenomenologically through neutron star cooling simulations [1, 53]. The small ${}^3\text{P}_2$ pairing gaps in Fig. 10 would imply that core neutrons are only superfluid at late times ($t \gtrsim 10^5 \text{ yrs}$).

3.5 Proton pairing

In neutron stars, matter is in beta equilibrium, with equal rates for neutrons undergoing beta decay and protons capturing electrons. As a result, matter in the interior of neutron stars at densities comparable to that of nuclear matter consists of $\sim 95\%$ neutrons and $\sim 5\%$ protons and electrons. Therefore, proton Fermi wave numbers are considerably lower than neutron ones, $k_F^p = k_F^n [x/(1-x)]^{1/3}$, where $x = n_p/n$ is the proton fraction. If only the free-space interaction contributed to pairing, protons in neutron stars would form a ${}^1\text{S}_0$ superfluid, unless proton densities high enough to favor ${}^3\text{P}_2$ pairing are reached.

Calculating proton pairing gaps is a challenging problem due to the coupling of protons to the denser neutron background. An important effect is that the proton effective mass, and therefore the density of states that enters the pairing strength in the exponent in the expression for the gap, is smaller than the neutron effective mass in neutron-rich matter, $m_p^* < m_n^*$ (see the general considerations in Fermi liquid theory in Ref. [54]). This decreases the proton ${}^1\text{S}_0$ gap significantly for a particular proton density, n_p , compared to the neutron gap for a neutron density equal to n_p [47, 55]. In addition to effective-mass effects, the coupling to the denser neutron background amplifies the repulsive contributions to the pairing interaction from three-nucleon forces and decreases the proton ${}^1\text{S}_0$ gap further [47, 55].

The situation regarding induced interactions is less clear. Refer-

ence [56] found induced interactions to be repulsive with a stronger reduction of the proton 1S_0 gap compared to the neutron one, whereas Ref. [55] found attractive induced interactions. A systematic study of proton pairing in neutron-rich matter incorporating the discussed many-body effects consistently remains an important outstanding problem.

4 The inner crust

From the calculations described above, one sees that pure neutron matter is expected to be paired in the 1S_0 state at neutron densities less than about $n_s/2$. However, in neutron stars one does not find bulk neutron matter at such densities, because this density range corresponds to the inner crust, in which the neutrons permeate a crystal lattice of neutron-rich nuclei. The inner crust of neutron stars, while making up only a small fraction of the mass of the star, is important for a variety of reasons (see, e.g., Ref. [57]). One is that heat from the interior of the star has to pass through this region on its way to the surface, and therefore the transport properties of the matter influence surface temperatures. Another reason is that a number of observed phenomena, including glitches in the rotation rate of pulsars and quasiperiodic oscillations observed in giant flares emitted by magnetized neutron stars, have been attributed to processes involving a neutron superfluid in the inner crust. Thus, it is necessary to understand the thermodynamic and transport properties of matter in the crust.

4.1 Static properties

Calculating the static properties is a formidable challenge for a number of reasons. As we have seen in earlier sections, even at the relatively low densities of interest in neutron star crusts, correlations are important. This means that in a mean-field calculation one must employ effective interactions rather than free-space ones. Typically, such interactions are fitted to observed properties of nuclei and to the calculated properties of pure neutron matter. Particularly popular choices are of the Skyrme form, which makes for computational simplicity, supplemented by a pairing interaction. In nuclear physics parlance, mean-field calculations with effective interactions are referred to as Hartree–Fock (HF) ones when pairing is neglected and as Hartree–Fock–Bogoliubov (HFB) ones when it is included. In the HFB calculations, one solves self-consistently for the functions $u_i(\mathbf{r})$ and $v_i(\mathbf{r})$ describing the particle and hole amplitudes for excitations in the state i . These two functions are the analogues of the quantities $u_{\mathbf{k}}$ and $v_{\mathbf{k}}$

for infinite matter.

To date, no HFB calculations that take into account the crystalline structure have been made and it is necessary to make further assumptions. A common one is to use what is referred to as the Wigner–Seitz approximation, in which one replaces the unit cell in coordinate space by a sphere of the same volume.⁸ To mimic the situation in a crystal, one applies boundary conditions at the edge of the Wigner–Seitz cell that allow the density there to remain nonzero, whereas for box boundary conditions the neutron density there would vanish. The present state of the art is described in Ref. [59] and a comparison of results for a variety of effective interactions is given in Ref. [60]. A simplified way of calculating pairing effects is to first perform a HF calculation for the normal state and then to include pairing in the spirit of the BCS theory for uniform matter, in which pairing occurs between particles in time-reversed single-particle states which, e.g., for S-wave pairing means particles with equal and opposite momentum and spin. We shall refer to this approximation as “HF+BCS”. More generally, pairing can occur between particles in states that are not related by time reversal: in an atomic nucleus pairing can occur between states with the same total orbital angular momentum, opposite projections of the orbital angular momentum and spin, but different radial quantum numbers, so-called “off-diagonal” pairing. The importance of these off-diagonal terms is well illustrated by calculations of the specific heat of matter in the inner crust [61]. In the HF+BCS approximation there is a single transition temperature to the paired state. However, in the inner crust, one has two rather different sorts of matter (the nuclei and the interstitial neutrons), and if coupling between the two components were small, one would expect there to be two transition temperatures, one corresponding to the matter in nuclei and the other corresponding to that for the outside neutrons. The HFB results indeed exhibit two maxima in the specific heat, corresponding to the transitions in the two sorts of matter.

4.2 Hydrodynamic equations

To describe dynamical processes for matter in the inner crust is generally complicated, but for long-wavelength and low-frequency phenomena one can adopt a hydrodynamic approach. Because of the presence of a neutron superfluid in the lattice of nuclei in the inner crust, the system has an extra degree of freedom compared with normal matter. Following Ref. [62], we now describe how one may develop a two-fluid description in which the system is regarded as being made up of a superfluid component and a normal component, as was previously done

⁸The name for this approximation stems from a similar approximation made in momentum space to simplify calculations of band structure [58].

for superfluid liquid ${}^4\text{He}$. While in the case of liquid ${}^4\text{He}$ the normal component corresponds to thermal excitations, for matter in the inner crust, the normal component is made up of the nuclei and electrons and so does not disappear at zero temperature. The system thus has similarities to dilute solutions of ${}^3\text{He}$ in ${}^4\text{He}$, where the ${}^3\text{He}$ atoms play the role of the normal component. The state of the system locally is specified by the density of neutrons, n_n , the density of protons, n_p , averaged over length scales large compared with the spacing between nuclei, and the velocity of nuclei (and of electrons which move with them to ensure local charge neutrality), together with an extra variable because of the new degree of freedom associated with the neutron superfluid, its velocity \mathbf{v}_n , which we now define.

Pairing in a Fermi superfluid at point \mathbf{r} is described by the amplitude $\langle \hat{\psi}_\uparrow(\mathbf{r})\hat{\psi}_\downarrow(\mathbf{r}) \rangle$, where $\hat{\psi}_\sigma(\mathbf{r})$ is the annihilation field operator for a neutron with spin projection σ at position \mathbf{r} , and $\langle \dots \rangle$ denotes a quantum-mechanical or, at nonzero temperature, a thermal average. For a superfluid at rest, the phase $2\varphi(\mathbf{r})$ of this amplitude is independent of position, while for a moving superfluid it depends on space. The presence of the lattice of nuclei results in rapid spatial variations on the scale of the nuclear spacing due to disturbances in the flow produced by the nuclei, whereas in a translationally invariant system the phase varies smoothly in space. Just as for single-electron wave functions in a periodic lattice, one may characterize states of the neutron superfluid in the crust by a crystal momentum \mathbf{k} such that the change of the phase $\varphi(\mathbf{r})$ when the spatial coordinate is displaced by a lattice vector \mathbf{R} is given by $\mathbf{k} \cdot \mathbf{R}/\hbar$. Alternatively, one may define a coarse-grained average phase, $\phi(\mathbf{r})$, the average of φ over a region in the vicinity of \mathbf{r} with dimensions large compared with the lattice spacing but small compared with other length scales in the problem, in which case $\mathbf{k} = \hbar\nabla\phi$. An analogous situation occurs for atomic Bose–Einstein condensates in optical lattices, artificial crystal lattices created by standing-wave laser beams [63].

To derive the expression for the current density of neutrons, we consider a system where there is no net current of the various species. Under a Galilean transformation to a reference frame moving with velocity $-\mathbf{v}$ with respect to the original one, the wave function of the nucleons is multiplied by a space-dependent factor $\exp\left(\sum_j im\mathbf{v} \cdot \mathbf{r}_j/\hbar\right)$, where the sum is over all nucleons.⁹ From the Galilean invariance of the system, the neutron-number current density in the new frame is given by

$$\mathbf{j}_n = n_n\mathbf{v}. \quad (31)$$

In this equation, both \mathbf{j}_n and n_n refer to coarse-grained average quan-

⁹For simplicity of exposition, we do not consider explicitly the electrons, which are relativistic.

ties, as described above for ϕ . On the other hand, the current may be calculated directly in terms of the variation of the phase of the pairing amplitude. Under the Galilean transformation, the coarse-grained phase ϕ of the pairing amplitude, which is independent of space in the original frame, acquires a space-dependent contribution $m\mathbf{v} \cdot \mathbf{r}/\hbar$, so one can rewrite the expression (31) as

$$\mathbf{j}_n = n_n \mathbf{v}_n, \quad (32)$$

where

$$\mathbf{v}_n = \frac{\hbar \nabla \phi}{m}. \quad (33)$$

As one can see from Eq. (32), the quantity \mathbf{v}_n is the average neutron velocity in this situation and, quite generally, it is the neutron superfluid velocity in a two-fluid model.

Now let us turn to the case where the nuclei are moving. In general, the velocity of the nuclei is given in terms of the displacement $\boldsymbol{\xi}$ of a nucleus by

$$\mathbf{v}_p = \frac{d\boldsymbol{\xi}}{dt}. \quad (34)$$

Due to neutron–proton interactions, the motion of the protons induces a current of neutrons, an effect often referred to as “entrainment”. In the literature on quantum liquids it corresponds to “backflow”. We first consider the case where the phase ϕ is independent of space. Phenomenologically one may write for the neutron current

$$\mathbf{j}_n = n_n^n (\mathbf{v}_p)_0, \quad (35)$$

where the parameter n_n^n , which in general is a function of \mathbf{v}_p , corresponds to the density of neutrons that move with the nuclei, and the subscript “0” on the velocity indicates that it is the velocity in the frame in which ϕ is independent of space. In the context of the two-fluid model for superfluids, this contribution corresponds to the *normal* component, which is why we give it the superscript n . Because the solid is generally anisotropic due to the presence of the crystal lattice, n_n^n is a second-rank tensor, but to simplify the discussion we shall treat it as a scalar. For small values of \mathbf{v}_p , we may take n_n^n to be independent of \mathbf{v}_p .

Next we perform a Galilean transformation to the frame moving with velocity $-\mathbf{v}$. The neutron current in the new frame is given by

$$\mathbf{j}_n = n_n^n (\mathbf{v}_p)_0 + n_n \mathbf{v}, \quad (36)$$

which we now express in terms of velocities measured in the new frame. The proton velocity in the new frame is given by

$$\mathbf{v}_p = (\mathbf{v}_p)_0 + \mathbf{v} \quad (37)$$

and the velocity \mathbf{v}_n by \mathbf{v} and therefore the neutron current density (36) is given by

$$\mathbf{j}_n = n_n \frac{\hbar \nabla \phi}{m} + n_n^n (\mathbf{v}_p - \mathbf{v}_n) = n_n^n \mathbf{v}_p + n_n^s \mathbf{v}_n, \quad (38)$$

where $n_n^s = n_n - n_n^n$ is referred to as the neutron superfluid number density. The first equality in (38) is analogous to the expression $\hat{\mathbf{p}} - e\mathbf{A}$ for the current operator for a charged particle in the presence of a vector potential, where $\hat{\mathbf{p}}$ is the momentum operator and \mathbf{A} is the vector potential. Thus we see that a difference between the velocities of the normal and superfluid components gives rise to a vector potential acting on the neutrons.

Equation (38) provides the foundation for a two-fluid description of motion of matter in the inner crust. We shall assume that frequencies of interest are much less than the electron plasma frequency, in which case the electron density is equal to the proton density. The long-wavelength dynamics of the system may thus be described in terms of the coarse-grained averages of the densities of neutrons and protons, n_n and n_p , and the velocities \mathbf{v}_n and \mathbf{v}_p . On time scales long compared with the time for weak interaction processes, the numbers of neutrons and protons are separately conserved. The equation for neutron number conservation is

$$\frac{\partial n_n}{\partial t} + \nabla \cdot \mathbf{j}_n = \frac{\partial n_n}{\partial t} + \nabla \cdot (n_n^n \mathbf{v}_p + n_n^s \mathbf{v}_n) = 0 \quad (39)$$

and that for proton number conservation is

$$\frac{\partial n_p}{\partial t} + \nabla \cdot \mathbf{j}_p = 0, \quad (40)$$

where the proton current density is given by

$$\mathbf{j}_p = n_p \mathbf{v}_p. \quad (41)$$

These must be supplemented by equations for the time derivatives of \mathbf{v}_n and \mathbf{v}_p . The rate of change of the phase ϕ is given by the Josephson relation

$$\frac{\partial \phi}{\partial t} = -\frac{\mu_n}{\hbar}, \quad (42)$$

where μ_n is the neutron chemical potential, which is related to the energy per unit volume E by the equation $\mu_n = \partial E / \partial n_n$.¹⁰ Thus, on taking the gradient of Eq. (42) one finds

$$m \frac{\partial \mathbf{v}_n}{\partial t} + \nabla \mu_n = 0, \quad (43)$$

¹⁰In Secs. 4.2 and 4.3, E denotes the energy per unit volume, not the energy.

The final equation is that for momentum conservation. The total momentum density \mathbf{g} is the sum of the neutron and proton momentum densities,

$$\mathbf{g} = m\mathbf{j}_n + m\mathbf{j}_p, \quad (44)$$

where we have neglected the contribution of the electrons. The latter is of order μ_e/mc^2 times the proton contribution and the electron chemical potential, μ_e , is less than 10% of the proton rest mass. Conservation of momentum is expressed by the relation

$$\frac{\partial \mathbf{g}}{\partial t} + \nabla \cdot \mathbf{P} = 0, \quad (45)$$

where \mathbf{P} is the momentum flux (stress) tensor.

4.3 Long-wavelength collective modes

As an application of the above equations, we consider long-wavelength, small-amplitude oscillations of the medium about a state in which the velocities are zero. For simplicity we consider a uniform medium that is homogeneous initially. We linearize Eqs. (39), (40), (43), and (45). To lowest order in the velocities the first two of these equations become

$$\frac{\partial n_n}{\partial t} + n_n^n \nabla \cdot \mathbf{v}_p + n_n^s \nabla \cdot \mathbf{v}_n = 0, \quad (46)$$

and

$$\frac{\partial n_p}{\partial t} + n_p \nabla \cdot \mathbf{v}_p = 0. \quad (47)$$

The neutron chemical potential is a function of the neutron and proton densities, and therefore changes of it are given by

$$\delta\mu_n = E_{nn}\delta n_n + E_{np}\delta n_p, \quad (48)$$

where $E_{ij} = \partial\mu_i/\partial n_j = \partial^2 E/\partial n_i \partial n_j$, and Eq. (43) becomes

$$m \frac{\partial \mathbf{v}_n}{\partial t} + E_{nn} \nabla n_n + E_{np} \nabla n_p = 0. \quad (49)$$

In the case of a solid, the momentum flux tensor contains contributions from elastic forces and to describe these it is convenient to use the nuclear displacement, $\boldsymbol{\xi}$, rather than the velocity \mathbf{v}_p . The change in the proton density is given by

$$\delta n_p = -n_p \nabla \cdot \boldsymbol{\xi}. \quad (50)$$

The momentum flux tensor has contributions from elastic distortions of the lattice as well as from changes in the neutron density. In neutron star crusts, matter is expected to be microcrystalline, and at

wavelengths longer than the typical size of the single-crystal domain, the medium behaves elastically as a uniform medium and the changes in the momentum flux tensor are given by

$$\delta P_{ij} = (n_n \delta \mu_n + n_p \delta \mu_p) \delta_{ij} - S \left(\frac{\partial \xi_i}{\partial x_j} + \frac{\partial \xi_j}{\partial x_i} - \frac{2\delta_{ij}}{3} \sum_{k=1}^3 \frac{\partial \xi_k}{\partial x_k} \right), \quad (51)$$

where S is the effective shear elastic constant.

Detailed calculations of collective modes have been carried out in a number of works [64, 65, 66] and here we shall summarize the results. For an isotropic medium, there are two transverse modes, corresponding to lattice phonons with two orthogonal polarizations, and two longitudinal modes. In the absence of neutron-proton interactions, there would be no entrainment, and the transverse phonons would have a velocity ¹¹

$$v_t = \sqrt{\frac{S}{mn_p}}, \quad (\text{No entrainment}) \quad (52)$$

while with neutron-proton interactions included the result is

$$v_t = \sqrt{\frac{S}{m(n_p + n_n^*)}}. \quad (\text{Superfluid neutrons}) \quad (53)$$

This result reflects the fact that the superfluid flow must be irrotational, $\nabla \times \mathbf{v}_n = 0$, and consequently only the normal density of the neutrons enters. By contrast, when the neutrons are in the normal state, all of them contribute to the relevant mass density and

$$v_t = \sqrt{\frac{S}{\rho}}, \quad (\text{Normal neutrons}) \quad (54)$$

where ρ is the total mass density, which is approximately $m(n_p + n_n)$ in the nonrelativistic limit. In the absence of neutron-proton interactions, the two longitudinal modes correspond to phonons in the lattice and phonons in the neutron superfluid (the Bogoliubov-Anderson mode) and they have velocities

$$v_p = \sqrt{\frac{n_p^2 E_{pp} + \frac{4}{3}S}{mn_p}}, \quad (\text{No neutron-proton interaction}) \quad (55)$$

and

$$v_n = \sqrt{\frac{n_n E_{nn}}{m}}, \quad (\text{No neutron-proton interaction}). \quad (56)$$

¹¹To realize the situation envisaged here, one must imagine that when the neutron-proton interaction is absent, the proton-proton interaction is increased so that pure proton nuclei are bound.

When entrainment is included but coupling between the nucleon densities in the two modes is neglected, the mass density associated with the lattice phonons increases and that associated with the phonons in the neutron superfluid decreases, thereby decreasing the velocities of both modes:

$$v_p = \sqrt{\frac{\mathcal{E}^{nn} + \frac{4}{3}S}{m(n_p + n_n^n)}}, \quad (\text{With entrainment but no hybridization}) \quad (57)$$

and

$$v_n = \sqrt{\frac{n_n^s E_{nn}}{m}}, \quad (\text{With entrainment but no hybridization}) \quad (58)$$

where

$$\mathcal{E}^{nn} = n_p^2 E_{pp} + 2n_p n_n^n E_{np} + (n_n^n)^2 E_{nn}. \quad (59)$$

Finally, when interactions between the densities of neutrons and protons in the two modes are included, the modes are hybridized and their velocities are given by

$$v_{\pm}^2 = \frac{v_n^2 + v_p^2}{2} \pm \sqrt{\left(\frac{v_n^2 - v_p^2}{2}\right)^2 + v_{np}^4}, \quad (60)$$

where

$$v_{np}^2 = \left(\frac{n_n^s}{n_n^n + n_p}\right)^{1/2} \frac{E_{nn} n_n^n + E_{np} n_p}{m}. \quad (61)$$

When the neutrons are normal, there is a single longitudinal mode, a sound wave, with velocity

$$v_{\text{sound}} = \sqrt{\frac{B + \frac{4}{3}S}{\rho}}, \quad (62)$$

where B is the bulk modulus,

$$B = n_n^2 E_{nn} + 2n_n n_p E_{np} + n_p^2 E_{pp}. \quad (63)$$

In Fig. 11 we give an example of a calculation of mode frequencies. As one sees from the figure, these depend rather strongly on the value of the neutron superfluid density, a topic which we take up in the following subsection.

Recently, the calculations of mode frequencies have been extended to shorter wavelengths [67]. An interesting conclusion of that work is that the body-centered-cubic lattice of ions, which has generally been assumed to be the ground state because it has the lowest Coulomb lattice energy, may be destabilized by the presence of neutrons between nuclei. The physical origin of the effect is that the neutrons

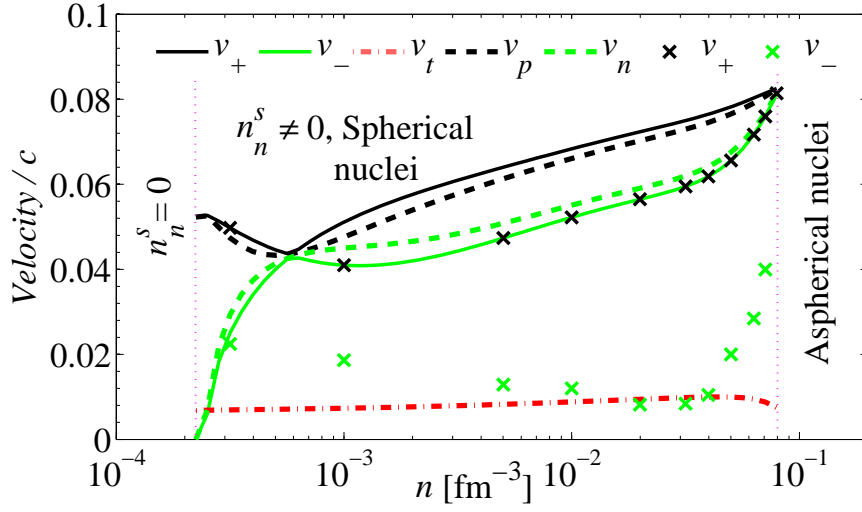


Figure 11: Velocities of long-wavelength modes as a function of nucleon density [66]. Velocities of modes when effects of entrainment are included are given by v_n and v_p when v_{np} is neglected, and by v_{\pm} when v_{np} is included. The velocity of the transverse modes is denoted by v_t . Curves are for $n_n^s = n^{\text{out}}$, the local density of neutrons outside nuclei, while the crosses show results for n_n^s taken from Chamel's calculation [69]. The derivatives E_{ij} were extracted from Lattimer and Swesty's equation of state calculations [68].

between nuclei give rise to an attractive induced interaction between nuclei which tends to favor inhomogeneous states in which regions of a high density of nuclei also have a high density of neutrons. This attraction is similar to the phonon-induced attraction between electrons that is responsible for superconductivity in metals and to the induced interactions between neutrons discussed in Sec. 2.1. The attraction is insufficient to cause instability at long wavelengths, but could be large enough to do so at shorter wavelengths where the other part of the nucleus–nucleus interaction, a Coulomb interaction screened by electrons, is reduced. We note that, while in the calculations of mode frequencies we have assumed that the neutrons are superfluid, the induced interaction would also be present if the neutrons are normal.

4.4 Band structure and the neutron superfluid density

Since the neutrons are subject to the periodic potential produced by the nuclei, the neutron spectra display a band structure. Even in the normal state, calculating the band structure of the system is very difficult, because the number of bands that are significantly occupied is of the order of half the number of neutrons per unit cell, the half being due to the spin degeneracy of the neutrons. This can be of order 10^3 , whereas in terrestrial condensed matter the number of bands considered for simple crystal structures is typically two orders of magnitude less. The large number of bands places extreme demands on the numerical accuracy required. The difficulty of performing band-structure calculations motivated the use of the Wigner-Seitz approximation described in Sec. 4.1. However, this approximation is inadequate to describe the effects of band structure on flow properties such as the neutron superfluid density, which is an important quantity for mode frequencies and for models of glitch phenomena based on a neutron superfluid moving relative to the lattice of nuclei in the crust: in both these cases the total moment of inertia of the superfluid neutrons is a crucial parameter. The difficulty in calculating the neutron superfluid density stems from the fact that the neutrons move in the periodic lattice of nuclei. Were it not for the lattice, the neutron superfluid density would be equal to the total density of neutrons. However, the medium is highly inhomogeneous on a microscopic scale, with nuclei containing nuclear matter with both protons and neutrons, and a neutron fluid between nuclei. Physically, one might expect that a good estimate of the neutron superfluid density would be the density of neutrons in the regions outside nuclei, n^{out} . However, as will be explained below, Chamel has performed band-structure calculations for neutrons in a lattice of nuclei, and finds the superfluid density to be an order of magnitude smaller [69]. We now describe some of the

issues relevant to calculating the superfluid density.

The quantity n_n^s represents the linear response of the current to a change in the gradient of the phase of the pairing amplitude. Let us begin by considering noninteracting particles moving in a periodic potential. The single-particle states are specified by a crystal momentum \mathbf{k} and a band index b , and the current density carried by the particles is¹²

$$\mathbf{j}_n = \frac{1}{\Omega} \sum_{\mathbf{k},b} f_{\mathbf{k},b} \mathbf{v}_{\mathbf{k},b}, \quad (64)$$

where $f_{\mathbf{k},b}$ is the particle distribution function, Ω is the volume of the system, and the current carried by a particle is its velocity,

$$\mathbf{v}_{\mathbf{k},b} = \nabla_{\mathbf{k}} \epsilon_{\mathbf{k},b}. \quad (65)$$

Here $\epsilon_{\mathbf{k},b}$ is the energy of the state with crystal momentum \mathbf{k} and band index b , and the sum is over all states within the first Brillouin zone.¹³ When an extra phase χ is applied to the single-particle states, the wave vector of the state is changed by an amount $\nabla\chi$. On the assumption that the change of the phase can be made adiabatically, the distribution function for the state \mathbf{k} after addition of the phase change is equal to that for the state $\mathbf{k} - \mathbf{q}$ initially, where $\mathbf{q} = \hbar\nabla\chi$ and the current density is given by

$$\mathbf{j}_n = \frac{1}{\Omega} \sum_{\mathbf{k},b} f_{\mathbf{k}-\mathbf{q},b} \mathbf{v}_{\mathbf{k},b} \simeq -\frac{1}{\Omega} \sum_{\mathbf{k},b} \mathbf{v}_{\mathbf{k},b} \mathbf{q} \cdot \nabla_{\mathbf{k}} f_{\mathbf{k},b}, \quad (66)$$

where we have assumed that the current vanishes in the initial state and the second expression holds for small \mathbf{q} . On writing $\nabla_{\mathbf{k}} f_{\mathbf{k},b} = (\partial f_{\mathbf{k},b} / \partial \epsilon_{\mathbf{k},b}) \nabla_{\mathbf{k}} \epsilon_{\mathbf{k},b} = (\partial f_{\mathbf{k},b} / \partial \epsilon_{\mathbf{k},b}) \mathbf{v}_{\mathbf{k},b}$ one finds

$$\mathbf{j}_n \simeq -\frac{1}{\Omega} \sum_{\mathbf{k},b} \mathbf{v}_{\mathbf{k},b} (\mathbf{q} \cdot \mathbf{v}_{\mathbf{k},b}) \frac{\partial f_{\mathbf{k},b}}{\partial \epsilon_{\mathbf{k},b}} = \frac{\mathbf{q}}{\Omega} \sum_{\mathbf{k},b} \frac{v_{\mathbf{k},b}^2}{3} \left(-\frac{\partial f_{\mathbf{k},b}}{\partial \epsilon_{\mathbf{k},b}} \right), \quad (67)$$

where the latter expression holds for isotropic matter and for crystals with cubic symmetry.¹⁴ The quantity

$$\frac{1}{\Omega} \sum_{\mathbf{k},b} \frac{v_{\mathbf{k},b}^2}{3} \left(-\frac{\partial f_{\mathbf{k},b}}{\partial \epsilon_{\mathbf{k},b}} \right) = \frac{1}{\Omega} \sum_{\mathbf{k},b} \frac{f_{\mathbf{k},b}}{3} \nabla_{\mathbf{k}}^2 \epsilon_{\mathbf{k},b} \quad (68)$$

has the dimensions of a number density divided by a mass. If one defines an effective mass by the relationship $1/m_{\mathbf{k},b}^{\text{eff}} = 1/3 \sum_i \partial^2 \epsilon_{\mathbf{k},b} / \partial k_i^2$,

¹²Note that, in this subsection, \mathbf{k} is a crystal momentum, not a wave vector.

¹³For simplicity, we do not indicate explicitly spin indices, which must also be summed over.

¹⁴For more complicated crystal structures the current is not generally in the direction of \mathbf{q} and the response is described by a tensor.

one sees that the quantity is the neutron density divided by the harmonic mean of the effective mass for occupied states. Fully occupied bands do not contribute to this quantity because of the periodicity of $\epsilon_{\mathbf{k},b}$ in \mathbf{k} space.

If neutrons are not superfluid, impurities in the lattice will transfer momentum to the lattice and the assumption that the neutrons adjust adiabatically to an imposed phase change will not hold. However, for a superfluid the assumption will be good, since pairing correlations maintain the coherent motion of the neutrons. To the extent that energies associated with pairing are small compared with other energies in the problem, such as the Fermi energy and band gaps, the response of the neutrons should be given approximately by the result (67). In that case, the neutron superfluid velocity is given by

$$\mathbf{v}_n = \frac{\mathbf{q}}{m}, \quad (69)$$

and therefore one sees that

$$n_n^s = \frac{m}{\Omega} \sum_{\mathbf{k},b} \frac{v_{\mathbf{k},b}^2}{3} \left(-\frac{\partial f_{\mathbf{k},b}}{\partial \epsilon_{\mathbf{k},b}} \right). \quad (70)$$

On replacing the distribution function by the zero temperature form $\Theta(\mu_n - \epsilon_{\mathbf{k}})$, where Θ is the Heaviside step function, one finds

$$n_n^s = \frac{1}{3} \int_{FS} \frac{m v_{\mathbf{k},b} \cdot d\mathbf{S}_{\mathbf{k}}}{(2\pi\hbar)^3}, \quad (71)$$

where the integral is to be carried out over the Fermi surface. The quantity $d\mathbf{S}_{\mathbf{k}}$ is an element of the area of the Fermi surface. For a spectrum $\epsilon_{\mathbf{k}} = k^2/2m_B$, where m_B is a parameter, Eq. (71) gives $n_n^s = (m/m_B)n_n$. If one writes the expression for the neutron current in the form $\mathbf{j}_n = \Xi \mathbf{q}$, the response function Ξ has the dimensions of a density divided by a mass. If one chooses the mass to be the bare neutron mass, one may regard a reduction of Ξ due to the periodic lattice as a reduction in the effective number of free neutrons. Alternatively, if one chooses some value for the density, a reduction of Ξ can be attributed to an increase in the effective mass of neutrons. To obtain a treatment that is close to the conventional one for the two-fluid model [70], it is convenient to choose as the mass the bare neutron mass and regard any reduction in Ξ as being a reduction of the number of superfluid neutrons compared with the total number. This choice of mass has the advantage that the expression for the current, Eq. (38), naturally involves the difference $\mathbf{v}_p - \mathbf{v}_n$: had we chosen a different mass \tilde{m} in the definition of the neutron velocity, Eq. (33), the uglier quantity $(\tilde{m}/m) \mathbf{v}_p - \mathbf{v}_n$ would appear instead. Of course, no physical results depend on the choice of the mass in the definition of the superfluid

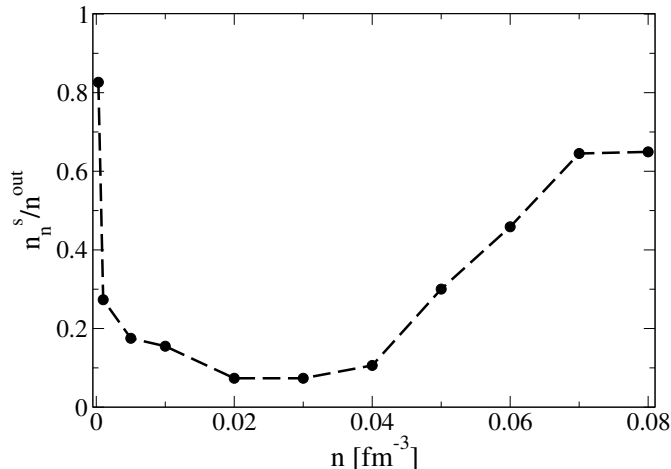


Figure 12: Neutron superfluid density n_n^s in terms of the density of neutrons outside nuclei, n^{out} , as a function of the total nucleon density n [69].

velocity, since the basic physical quantity of interest is the superfluid momentum per particle, $\hbar\nabla\phi$, as has been stressed in Ref. [71]. The traditional treatment brings out directly the fact that there is a single parameter, n_n^s , that describes the flow of the superfluid, whereas if one works in terms of momenta per particle, the currents are related to the momenta per particle by a tensor.

We now turn to Chamel's calculations [69]. He calculated in the Hartree–Fock approximation the band structure of neutrons moving in a body-centered-cubic lattice of nuclei. In Fig. 12 we show Chamel's results for n_n^s/n^{out} as a function of the total density of matter. Are there other physical effects which could change this result significantly? A basic assumption in using the result (71) is that pairing correlations have only a small effect on the neutron excitations. This is presumably a reasonable assumption provided the pairing gap Δ is small compared with splittings between single-neutron states produced by the periodic lattice. We know of no published numerical values of these splittings, but plots of neutron spectra are shown in Figs. 2-4 of Ref. [69]. At a density of 0.0003 fm^{-3} , which corresponds to a mass density $\sim 5 \times 10^{11} \text{ g cm}^{-3}$, slightly larger than the neutron drip density, the bands are very similar to those of free neutrons and splittings are of order 0.1 MeV. At a density 0.03 fm^{-3} (Fig. 3 of Ref. [69]), the band structure is complicated and it is difficult to resolve the splittings, while at a density of 0.08 fm^{-3} , close to the inner edge of the crust, the bands are again free-neutron like and splittings are of order 1 MeV. Pairing gaps in neutron matter at densities of order $n_s/10$ are typically of order 1 MeV which is similar in magnitude to splittings due to band structure: this indicates that pairing

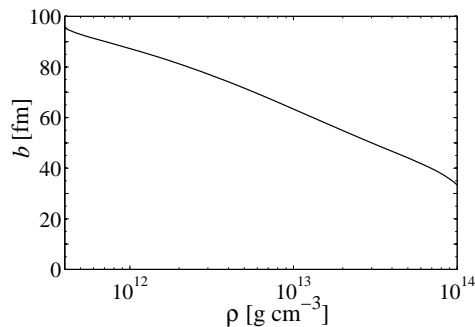


Figure 13: Lattice spacing b of the body-centered-cubic crystal in the inner crust as a function of the total matter density (from Ref. [67], which was based on the calculations of Ref. [68]).

could have a large effect on the band structure. Pairing reduces the effects of band structure because the pairing gap increases the size of energy denominators for processes in which neutron quasiparticles are scattered by the periodic lattice.

Another useful way to assess the importance of various effects is to estimate basic length scales. One important length is the separation between nuclei, and we show in Fig. 13 a plot of the lattice spacing of the body-centered-cubic cell in the neutron star crust as a function of the total density of nucleons. Another relevant length is the coherence length for the pairing correlations, ξ_{coh} , which is a measure of the size of a Cooper pair. In BCS theory this is given for uniform matter by

$$\xi_{\text{coh}} = \frac{\hbar v_F}{\pi \Delta} \approx \frac{63 \text{ MeV}}{\Delta} \frac{v_F}{c} \text{ fm}, \quad (72)$$

where v_F is the Fermi velocity. Thus, in the density range where the pairing gap for neutrons reaches its maximum value (~ 1 MeV), the coherence length is of order 10 fm, which is considerably less than the lattice spacing, while for neutron densities for which the gap is of order 0.1 MeV or less, it becomes larger than the lattice spacing. These estimates suggest that in the density range where the calculations of n_n^s based on the normal state band structure predict a strong reduction, correlated pairs of neutrons have a size much less than the lattice spacing and therefore neutron excitations propagate between scatterings from nuclei in the lattice not as free particles, but as the elementary excitations of the neutron superfluid.

Another effect that could play a role is the zero-point and thermal motion of the lattice, which will smear out in space the potential due to nuclei and thereby reduce scattering from the lattice. The smearing is described by the Debye–Waller factor and preliminary estimates indicate that the effect could be important [66].

5 Conclusion

During the past two decades, considerable progress has been made in understanding 1S_0 pairing in neutron matter. The impetus for these advances has come from a number of sources. One is that the experimental realization of degenerate gases of fermionic atoms led to the rediscovery of the work of Gor'kov and Melik-Barkhudarov [20], which showed that induced interactions play an important role even in the limit of low density. Their analytical results, together with the development of quantum Monte Carlo methods for solving the many-body problem have resulted in a reliable, quantitative understanding of gaps in neutron matter at low densities.

At higher densities there are significant uncertainties in the gap because, with increasing density, non-central components of nucleon-nucleon interactions become more important, thereby making the many-body problem more difficult to solve. In addition, three- and higher-body forces come into play. It is, for example, difficult to predict the density at which the neutron 1S_0 gap vanishes. In the future, one may anticipate that the development of quantum Monte Carlo methods, as well as of improved effective interactions, will make for more precise estimates. Even more uncertain than the 1S_0 gap are estimates for the 3P_2 gap (if any) because this, unlike the 1S_0 gap, which depends on the average of the pairing interaction over the Fermi surface, depends on *departures* of the pairing interaction from its average value. In addition, 3P_2 is a viable pairing channel only at densities around nuclear saturation density or above, where the many-body problem is difficult to solve and nuclear interactions are less constrained. Predicting pairing gaps for protons is bedevilled by the fact that the protons are a minority component in neutron star matter, and consequently induced interactions due to the surrounding neutrons play a large, but poorly understood, role.

Long-wavelength phenomena may be described in terms of a two-fluid model similar to the standard one for the helium liquids, but generalized to include the elastic effects of the crystal lattice. With improved effective interactions to describe nuclear properties, the road is now open to better determinations of the parameters entering the two-fluid model. Of particular importance for improved calculations of mode frequencies is a better understanding of the neutron superfluid density, and here a deeper study of the combined effects of pairing and band structure is called for. Properties of collective modes at shorter wavelengths are of interest for thermal and transport properties, but to date little work has been done on this problem.

Acknowledgments

We thank Joe Carlson, Nicolas Chamel, Kai Hebeler, Dmitry Kobyakov, and Alessandro Pastore for helpful input and discussions. This work was supported in part by the Natural Sciences and Engineering Research Council of Canada, the ERC Grant No. 307986 STRONGINT, the Helmholtz Association through the Helmholtz Alliance Program, contract HA216/EMMI “Extremes of Density and Temperature: Cosmic Matter in the Laboratory”, and the NewCompStar network, COST Action MP1304.

References

- [1] Page, D., Lattimer, J. M., Prakash, M., and Steiner, A. W. in *Novel Superfluids: Volume 2*. Eds. Bennemann, K. H. and Ketterson, J. B., Oxford University Press, Oxford (2014), p. 505 [arXiv:1302.6626].
- [2] Lombardo, U. and Schulze, H.-J. Superfluidity in neutron star matter. In *Physics of Neutron Star Interiors*, eds. Blaschke, D., Glendenning, N. K., and Sedrakian, A. Lecture Notes in Physics **578**, 30 (2001).
- [3] Dean, D. J. and Hjorth-Jensen, M. Pairing in nuclear systems: From neutron stars to finite nuclei, *Rev. Mod. Phys.* **75**, 607 (2003).
- [4] Bohr, A., Mottelson, B. R., and Pines, D. Possible analogy between the excitation spectra of nuclei and those of the superconducting metallic state. *Phys. Rev.* **110**, 936 (1958).
- [5] Brink, D. M. and Broglia, R. A. *Nuclear Superfluidity: Pairing in Finite Systems*. Oxford University Press, Oxford (2005).
- [6] Migdal, A. B. Superfluidity and the moments of inertia of nuclei. *Zh. Eksp. Teor. Fiz.* **37** 249 (1959) [*Sov. Phys. JETP* **10**, 176 (1960)]; *Nucl. Phys.* **13**, 655 (1959).
- [7] Ginzburg, V. L. and Kirzhnits, D. A. On the superfluidity of neutron stars. *Zh. Eksp. Teor. Fiz.* **47**, 2006 (1964) [*Sov. Phys. JETP* **20**, 1346 (1965)].
- [8] Ginzburg, V. L. Superfluidity and superconductivity in the Universe. *Usp. Fiz. Nauk* **97**, 601 (1969) [*Sov. Phys.-Uspekhi* **12**, 241 (1969)]; *J. Stat. Phys.* **1**, 3 (1969).
- [9] Baym, G., Pethick, C. J., and Pines, D. Superfluidity in neutron stars. *Nature* **224**, 673 (1969).

- [10] Hoffberg, M., Glassgold, A. E., Richardson, R. W., and Ruderman, M. Anisotropic superfluidity in neutron star matter. *Phys. Rev. Lett.* **24**, 775 (1970).
- [11] Stoks, V. G. J., Klomp, R. A. M., Rentmeester, M. C. M., and de Swart, J. J. Partial-wave analysis of all nucleon-nucleon scattering data below 350 MeV. *Phys. Rev. C*, **48**, 792 (1993).
- [12] Clark, J. W., Davé, R. D., and Chen, J. M. C. Nucleonic superfluids. In *Condensed Matter Theories, Vol. 8*, Plenum, New York (1993); see also Chen, J. M. C., Clark, J. W., Davé, R. D., and Khodel, V. V. Pairing gaps in nucleonic superfluids. *Nucl. Phys. A* **555**, 59 (1993).
- [13] Wambach, J., Ainsworth, T. L., and Pines, D. Quasiparticle interactions in neutron matter for applications in neutron stars. *Nucl. Phys. A* **555**, 128 (1993).
- [14] de Gennes, P. G. *Superconductivity of Metals and Alloys*. Westview Press, Boulder (1966).
- [15] Tinkham, M. *Introduction to Superconductivity*. McGraw-Hill, New York (1996).
- [16] Wiringa, R. B., Stoks, V. G. J., and Schiavilla, R. Accurate nucleon-nucleon potential with charge-independence breaking. *Phys. Rev. C* **51**, 38 (1995).
- [17] Khodel, V. A., Khodel, V. V., and Clark, J. W. Solution of the gap equation in neutron matter. *Nucl. Phys. A* **598**, 390 (1996).
- [18] Gezerlis, A. and Carlson, J. Strongly paired fermions: Cold atoms and neutron matter. *Phys. Rev. C* **77**, 032801(R) (2008); Gezerlis, A. and Carlson, J. Low-density neutron matter. *Phys. Rev. C* **81**, 025803 (2010).
- [19] For reviews, see Bloch, I., Dalibard, J., and Zwerger, W. Many-body physics with ultracold gases. *Rev. Mod. Phys.* **80**, 885 (2008); Giorgini, S., Pitaevskii, L. P., and Stringari, S. Theory of ultracold atomic Fermi gases. *Rev. Mod. Phys.* **80**, 1215 (2008).
- [20] Gor'kov, L. P. and Melik-Barkhudarov, T. K. Contribution to the theory of superfluidity in an imperfect Fermi gas. *Zh. Eksp. Teor. Fiz.* **40**, 1452 (1961) [*Sov. Phys. JETP* **13**, 1018 (1961)].
- [21] Heiselberg, H., Pethick, C. J., Smith, H., and Viverit, L. Influence of induced interactions on the superfluid transition in dilute Fermi gases. *Phys. Rev. Lett.* **85**, 2418 (2000).

- [22] Berk, N. F. and Schrieffer, J. R. Effect of ferromagnetic spin correlations on superconductivity. *Phys. Rev. Lett.* **17**, 433 (1966).
- [23] Anderson, P. W. and Brinkman, W. F. Anisotropic superfluidity in ^3He : A possible interpretation of its stability as a spin-fluctuation effect. *Phys. Rev. Lett.* **30**, 1108 (1973).
- [24] Martikainen, J.-P., Kinnunen, J. J., Törmä, P., and Pethick, C. J. Induced interactions and the superfluid transition temperature in a three-component Fermi gas. *Phys. Rev. Lett.* **103**, 260403 (2009).
- [25] Bertsch, G. F. *The Many-Body Challenge Problem (MBX)*. See Bishop, R. F. *Int. J. Mod. Phys. B* **15**, 10, iii (2001).
- [26] Carlson, J., Gandolfi, S., and Gezerlis, A. Quantum Monte Carlo approaches to nuclear and atomic physics. *Prog. Theor. Exp. Phys.* 01A209 (2012).
- [27] See, e.g., Pethick, C. J. and Smith, H. *Bose–Einstein Condensation in Dilute Gases*, 2nd ed., Cambridge University Press, Cambridge (2008), Sec. 17.3.1.
- [28] Schwenk, A. and Pethick, C. J. Resonant Fermi gases with a large effective range *Phys. Rev. Lett.* **95**, 160401 (2005).
- [29] Bogner, S. K., Kuo, T. T. S., and Schwenk, A. Model independent low momentum nucleon interaction from phase shift equivalence. *Phys. Rept.* **386**, 1 (2003).
- [30] Hebeler, K., Schwenk, A., and Friman, B. Dependence of the $^1\text{S}_0$ superfluid pairing gap on nuclear interactions. *Phys. Lett. B* **648**, 176 (2007).
- [31] Hebeler, K., and Schwenk, A. Chiral three-nucleon forces and neutron matter. *Phys. Rev. C* **82**, 014314 (2010).
- [32] Zuo, W., Li, Z. H., Lu, G. C., Li, J. Q., Scheid, W., Lombardo, U., Schulze, H. J., and Shen, C. W. $^1\text{S}_0$ proton and neutron superfluidity in beta stable neutron star matter. *Phys. Lett. B* **595**, 44 (2004).
- [33] Baldo, M., Elgarøy, Ø., Engvik, L., Hjorth-Jensen, M., and Schulze, H.-J. $^3\text{P}_2$ – $^3\text{F}_2$ pairing in neutron matter with modern nucleon-nucleon potentials. *Phys. Rev. C* **58**, 1921 (1998).
- [34] Foulkes, W. M. C., Mitas, L., Needs, R. J., and Rajagopal, G. Quantum Monte Carlo simulations of solids. *Rev. Mod. Phys.* **73**, 33 (2001).

- [35] Ceperley, D. M. and Alder, B. J. Ground state of the electron gas by a stochastic method. *Phys. Rev. Lett.* **45**, 566 (1980).
- [36] Pieper, S. C. Quantum Monte Carlo calculations of light nuclei. *Riv. Nuovo Cim.* **31**, 709 (2008).
- [37] von der Linden, W. A quantum Monte Carlo approach to many-body physics. *Phys. Rep.* **220**, 53 (1992); Koonin, S. E., Dean, D. J., and Langanke, K. Shell model Monte Carlo methods. *Phys. Rep.* **278**, 1 (1997); Schmidt, K. E. and Fantoni, S. A quantum Monte Carlo method for nucleon systems. *Phys. Lett. B* **446**, 99 (1999).
- [38] Stratonovich, R. L. On a method of calculating quantum distribution functions. *Dokl. Akad. Nauk. SSSR* **115**, 1097 (1957) [*Sov. Phys. Doklady* **2**, 416 (1957)]; Hubbard, J. Calculation of partition functions. *Phys. Rev. Lett.* **3**, 77 (1959).
- [39] Carlson, J., Chang, S.-Y., Pandharipande, V. R., and Schmidt, K. E. Superfluid Fermi gases with large scattering length. *Phys. Rev. Lett.* **91**, 050401 (2003).
- [40] Fabrocini, A. Fantoni, S., Illarionov, A. Yu., and Schmidt, K. E. Superfluid phase transition in neutron matter with realistic nuclear potentials and modern many-body theories. *Phys. Rev. Lett.* **95**, 192501 (2005); Gandolfi, S., Illarionov, A. Yu., Fantoni, S., Pederiva, F. and K. E. Schmidt, Equation of state of superfluid neutron matter and the calculation of the 1S_0 pairing gap. *Phys. Rev. Lett.* **101**, 132501 (2008); Gandolfi, S., Illarionov, A. Yu., Pederiva, F., Schmidt, K. E., and Fantoni, S. Equation of state of low-density neutron matter, and the 1S_0 pairing gap. *Phys. Rev. C* **80**, 045802 (2009).
- [41] Shankar, R. Renormalization group approach to interacting fermions. *Rev. Mod. Phys.* **66**, 129 (1994).
- [42] Schwenk, A., Friman, B., and Brown, G. E. Renormalization group approach to neutron matter: Quasiparticle interactions, superfluid gaps and the equation of state. *Nucl. Phys. A* **713**, 191 (2003).
- [43] Gubbels, K. B. and Stoof, H. T. C. Renormalization group theory for the imbalanced Fermi gas. *Phys. Rev. Lett.* **100**, 140407 (2008).
- [44] Floerchinger, S., Scherer, M., Diehl, S., and Wetterich, C. Particle-hole fluctuations in the BCS-BEC crossover, *Phys. Rev. B* **78**, 174528 (2008).

- [45] Schwenk, A. Superfluidity in neutron stars and cold atoms, *AIP Conf. Proc.* **892**, 502 (2007).
- [46] Cao, L. G., Lombardo, U., and Schuck, P. Screening effects in superfluid nuclear and neutron matter within Brueckner theory. *Phys. Rev. C* **74**, 064301 (2006).
- [47] Zhou, X.-R., Schulze, H.-J., Zhao, E.-G., Pan, F., and Draayer, J. P. Pairing gaps in neutron stars. *Phys. Rev. C* **70**, 048802 (2004).
- [48] Khodel, V. A., Clark, J. W., Takano, M., and Zverev, M. V. Phase transitions in nucleonic matter and neutron-star cooling, *Phys. Rev. Lett.* **93**, 151101 (2004).
- [49] Dong, J. M., Lombardo, U., and Zuo, W. ${}^3\text{PF}_2$ pairing in high-density neutron matter, *Phys. Rev. C* **87**, 062801 (2013).
- [50] Pethick, C. J. and Ravenhall, D. G. Nuclear physics of dense matter. *Ann. N.Y. Acad. Sci.* 647, 503 (1991).
- [51] Schwenk, A. and Friman, B. Polarization contributions to the spin dependence of the effective interaction in neutron matter. *Phys. Rev. Lett.* **92**, 082501 (2004).
- [52] Hammer, H.-W., Nogga, A., and Schwenk, A. Three-body forces: From cold atoms to nuclei, *Rev. Mod. Phys.* **85**, 197 (2013).
- [53] Yakovlev D. G. and Pethick, C. J. Neutron star cooling. *Ann. Rev. Astron. Astrophys.* **42**, 169 (2004).
- [54] Sjöberg, O. On the Landau effective mass in asymmetric nuclear matter. *Nucl. Phys. A* **265**, 511 (1976).
- [55] Baldo, M. and Schulze, H.-J. Proton pairing in neutron stars. *Phys. Rev. C* **75**, 025802 (2007).
- [56] Wambach, J., Ainsworth, T. L., and Pines, D. in *Neutron Stars: Theory and Observation*. Eds. Ventura, J. and Pines, D., Dordrecht: Kluwer (1991), p. 37.
- [57] Haensel, P., Potekhin, A.Y., and Yakovlev, D. G. *Neutron Stars I Equation of State and Structure*, Springer, New York (2007).
- [58] Wigner, E. and Seitz, F. On the constitution of metallic sodium. *Phys. Rev.* **43**, 804 (1933).
- [59] Pastore, A., Baroni, S., and Losa, C. Superfluid properties of the inner crust of neutron stars. *Phys. Rev. C* **84**, 065807 (2011).

- [60] Pastore, A., Margueron, J., Schuck, P., and Viñas, X. Pairing in exotic neutron-rich nuclei near the drip line and in the crust of neutron stars. *Phys. Rev. C* **88**, 034314 (2013).
- [61] Pastore, A. Superfluid properties of the inner crust of neutron stars. II. Wigner-Seitz cells at finite temperature. *Phys. Rev. C* **86**, 065802 (2012).
- [62] Pethick, C. J., Chamel, N., and Reddy, S. Superfluid dynamics in neutron star crusts. *Prog. Theor. Phys. Suppl.* **186**, 9 (2010).
- [63] Krämer, M., Pitaevskii, L., and Stringari, S. Macroscopic dynamics of a trapped Bose-Einstein condensate in the presence of 1D and 2D optical lattices. *Phys. Rev. Lett.* **88**, 180404 (2002); Machholm, M., Pethick, C. J., and Smith, H. Band structure, elementary excitations, and stability of a Bose-Einstein condensate in a periodic potential. *Phys. Rev. A* **67**, 053613 (2003).
- [64] Cirigliano, V., Reddy, S., and Sharma, R. Low-energy theory for superfluid and solid matter and its application to the neutron star crust. *Phys. Rev. C* **84**, 045809 (2011).
- [65] Chamel, N., Page, D., and Reddy, S. Low-energy collective excitations in the neutron star inner crust. *Phys. Rev. C* **87**, 035803 (2013).
- [66] Kobyakov, D. and Pethick, C. J. Dynamics of the inner crust of neutron stars: Hydrodynamics, elasticity, and collective modes. *Phys. Rev. C* **87**, 055803 (2013).
- [67] Kobyakov, D. and Pethick, C. J. Towards a metallurgy of neutron star crusts. *Phys. Rev. Lett.* **112**, 112504 (2014).
- [68] Lattimer, J. M. and Swesty, F. D. A generalized equation of state for hot, dense matter. *Nucl. Phys. A*, **535**, 331 (1991) and the website www.astro.sunysb.edu/dswesty/lseos.html.
- [69] Chamel, N. Neutron conduction in the inner crust of a neutron star in the framework of the band theory of solids. *Phys. Rev. C* **85**, 035801 (2012).
- [70] Landau, L. D. and Lifshitz, E. M. *Course of Theoretical Physics, Vol. 6, Fluid Mechanics*, 2nd ed., Pergamon, Oxford (1987), p. 139.
- [71] Chamel, N. and Haensel, P. Entrainment parameters in a cold superfluid neutron star core. *Phys. Rev. C* **73**, 045802 (2006).